

We are IntechOpen, the world's leading publisher of Open Access books Built by scientists, for scientists

5,000

Open access books available

125,000

International authors and editors

140M

Downloads

Our authors are among the

154

Countries delivered to

TOP 1%

most cited scientists

12.2%

Contributors from top 500 universities



WEB OF SCIENCE™

Selection of our books indexed in the Book Citation Index
in Web of Science™ Core Collection (BKCI)

Interested in publishing with us?
Contact book.department@intechopen.com

Numbers displayed above are based on latest data collected.
For more information visit www.intechopen.com



Wideband Wearable Antennas for 5G, IoT, and Medical Applications

Albert Sabban

Abstract

Wearable compact antennas are a major part of every wearable 5G communication system, IoT, and biomedical systems. Several types of printed antennas are employed as wearable antennas. Printed dipole, microstrip antennas, printed loops, slot antennas, and PIFA antennas are employed as wearable antennas. Compact efficient antennas significantly affect the electrical performance of wearable communication systems. In several communication and medical systems, the polarization of the received signal is not known. The polarization of the received signal may be vertical, horizontal, or circular polarized. In these systems, it is crucial to use dual-polarized receiving antennas. The antennas presented in this chapter may be linearly or dually polarized. Design trade-offs, simulation results, and measured results on human body of small wideband printed antennas with high efficiency are presented in this chapter. For example, the low-volume dually polarized antenna dimensions are $50 \times 50 \times 0.5$ mm. The antenna beamwidth is around 100° . The antennas gain is around 0–4 dBi. Metamaterial technology is used to improve the electrical performance of wearable antennas. The proposed antennas may be used in wearable wireless communication and medical RF systems. The antennas' electrical performance on human body is presented in this chapter.

Keywords: wearable antennas, 5G communication system, IoT, biomedical systems, metamaterial technology, metamaterial antennas, microstrip antennas

1. Introduction

Microstrip antennas are widely used in communication system and seekers. Microstrip antennas possess attractive features that are crucial to 5G communication, IoT, and medical systems. These antennas are compact, flexible, lightweight, and relatively cheap. In addition, we can integrate the RF modules with the antennas on the same substrate. Printed antennas have been widely presented in the literature in the last 20 years [1–9]. Electromagnetic fields' transmission losses of human tissues have been investigated in the papers [10, 11]. However, the effect of human body on the impedance and efficiency of wearable antennas was not always presented [12, 13]. Printed wearable antennas have been presented in the last 10 years [1–20]. A review of wearable antennas designed and developed for several applications at different frequencies over the last 10 years is listed [15]. Wearable meander line antennas are presented in [12]. These antennas function in the frequency range between 750 and 2600 MHz. A textile antenna performance near human body is presented at 2.4 GHz, see [13]. The effect of human body on

portable RF antennas is studied in [16]. In this chapter, the authors determine that the antennas' length in free space is larger by 10–20% from the length of wearable antennas. Measurement of the antenna gain in this paper shows that a wide dipole (1.16×0.1 m) has -13 dBi gain. Wearable antennas for cellular applications are presented in [12–16]. Electrical specifications of medical devices are different from the electrical specifications for cellular devices. Medical wearable sensors are presented in [21–48]. Wearable devices support the development of personal medical sensors and systems with real-time response to help improve patient's health. Wearable medical sensors and devices can measure the sweat rate, body temperature, heartbeat, and blood pressure, perform gait analysis, and measure other body health parameters of the patient wearing these sensors, see Refs. [21–49]. In this chapter, novel wideband compact wearable antennas for 5G communication and medical systems are presented. Numerical results in free space and near the human body are presented.

2. Printed wearable antennas for 5G and medical applications

Wearable antennas should be compact, have lightweight, are low cost, and are flexible. Microstrip antennas, printed loops, printed dipoles, slot antennas, and PIFA antennas are compact, low cost, conformable, and have lightweight. These antennas are a good choice to be employed as wearable antennas for IoT and medical applications.

Applications of wearable antennas:

- 5G Communication Systems
- Medical
- Wireless Communication
- IoT
- WLAN
- HIPER LAN
- GPS
- Military Applications

2.1 Double-layer printed wearable dipole antennas

Single-layer printed dipole antennas have a narrow bandwidth less than 1% for VSWR better than 2:1. The length of the dipole may be between quarter wavelength to half wavelength. The antenna directivity is around 0 dBi and the beam width is around 90° – 100° . The antenna bandwidth may be improved by printing the antenna feed network on a dielectric substrate and by printing the radiating dipole on a second layer. The electromagnetic fields are coupled to the radiating dipole. The bandwidth of the double-layer printed dipole may be between 1 and 5% for VSWR better than 2:1 as a function of the dipole configuration and the layers thickness. The printed dipole antenna consists of two layers. The first layer consists of a 0.8-mm substrate with 3.5 as dielectric constant. The second layer consists of a 0.8-mm substrate with 2.2 as dielectric constant. The substrate thickness

determines the antenna bandwidth. However, thinner antennas are flexible. The antenna dimensions are designed to operate on the patient's body by using electromagnetic software [50]. The double-layer antenna is shown in **Figure 1**. The directivity of the antenna at 420 MHz is around 4 dBi as shown in **Figure 2**.

A double-layer 460 MHz dipole antenna is shown in **Figure 3**. The antenna dimensions are 20×4 cm. The directivity of the antenna at 460 MHz is around 5 dBi as presented in **Figure 4**. The antenna beamwidth is around 120° .

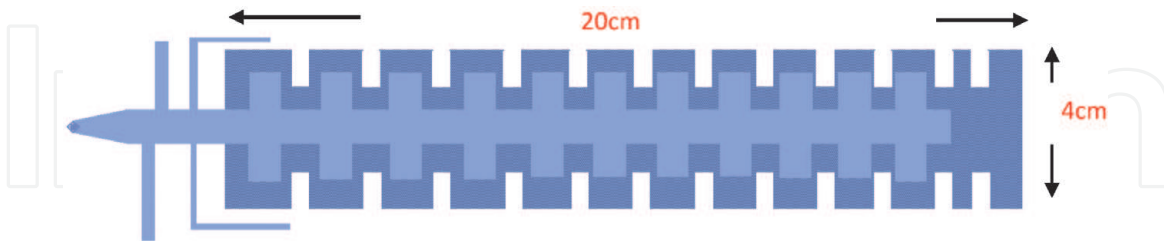


Figure 1.
 Wearable double-layer 420 MHz printed dipole antenna.

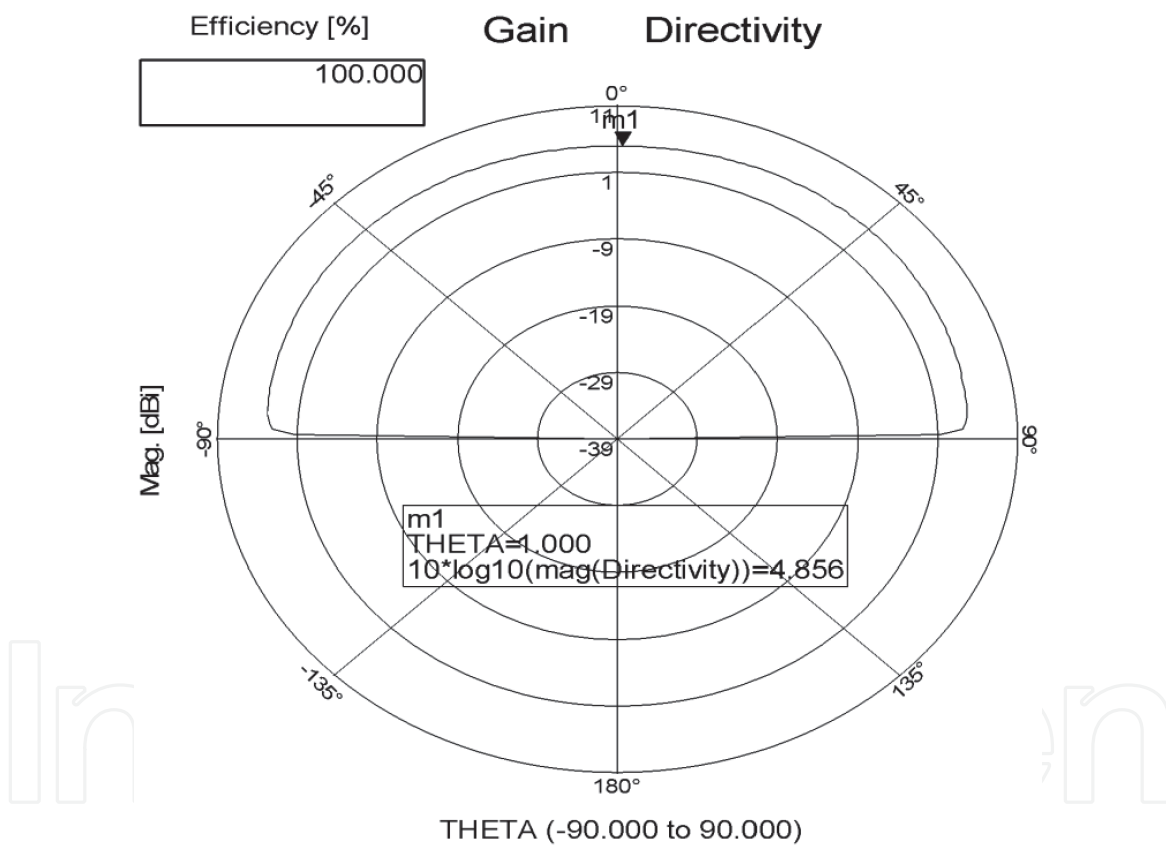


Figure 2.
 Radiation pattern of a wearable double-layer printed dipole antenna.

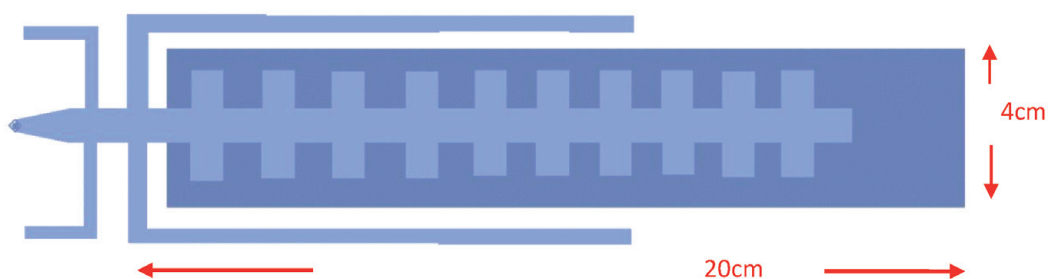


Figure 3.
 Wearable double-layer 460 MHz printed dipole antenna.

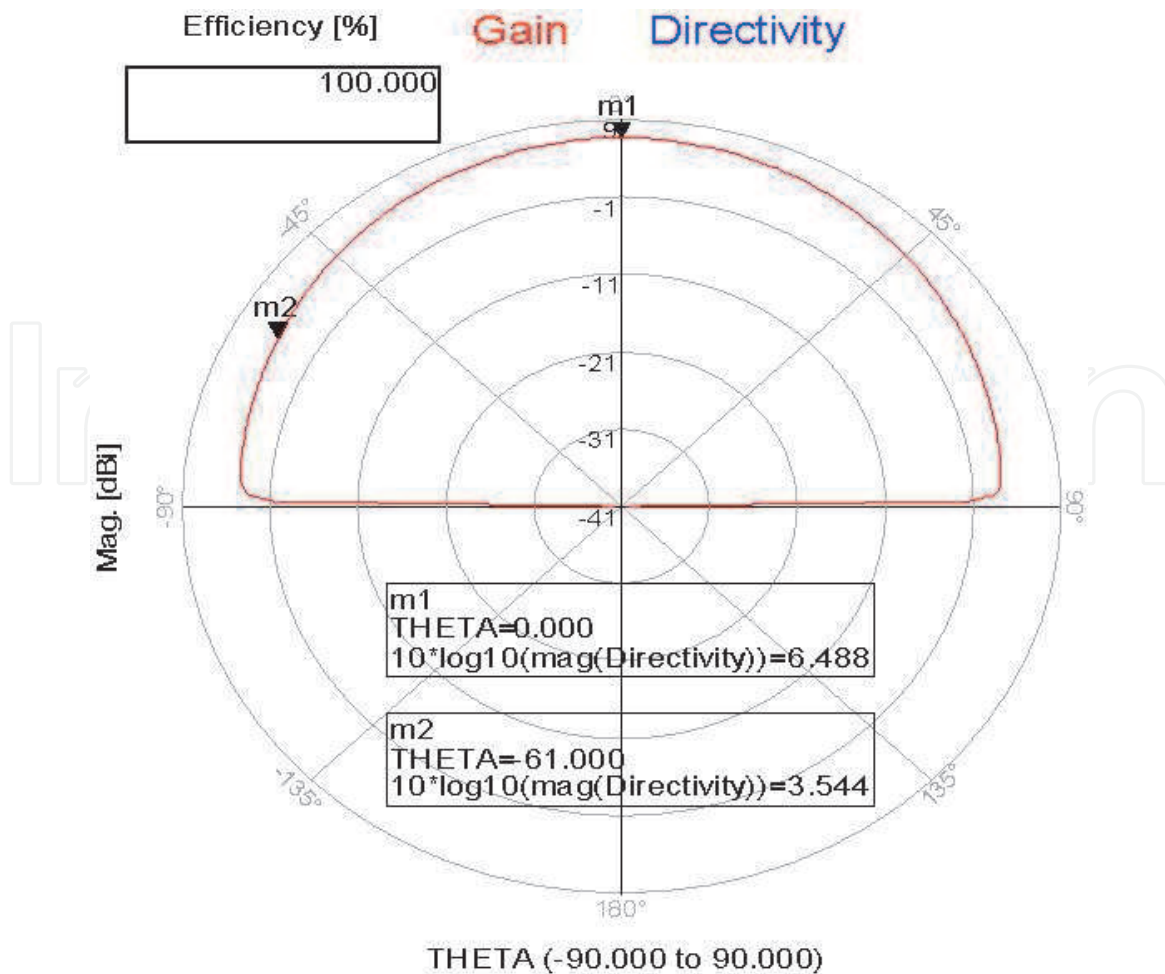


Figure 4.
Radiation pattern of a wearable double-layer printed dipole at 460 MHz.

3. Printed wearable dual-polarized dipole antennas

In several communication and medical systems, the polarization of the received signal is not known. The polarization of the received signal may be vertical, horizontal, or circular polarized. In these systems, it is crucial to use dual-polarized receiving antennas. Two wearable antennas are presented in this section; the first is a dual-polarized printed dipole. The second antenna is a dual-polarized, folded, printed microstrip dipole. The compact, printed, loaded dipole antenna is horizontally polarized. The antenna dimensions have been designed to operate on the patient's body by employing electromagnetic software [50]. The antenna consists of two layers. The first layer consists of a 0.08-cm dielectric substrate with 3.5 as relative dielectric constant. On this layer, the antenna feed network is printed. The radiating elements are printed on the second layer which consists of a 0.08-cm dielectric substrate with 2.2 as relative dielectric constant. Thicker antennas have a wider bandwidth. However, thinner antennas are more flexible with a narrower bandwidth. The printed slot antenna is vertically polarized. The printed dipole and the slot antenna provide dual orthogonal polarizations. The wearable antenna current distribution and dimensions are shown in **Figure 5**.

The radiating dipole dimensions are $21 \times 4 \times 0.16$ cm. The wearable antenna may be employed in medical and IoT systems. The antenna may be attached to the patient clothes, in the front or in the back zone. The antenna has been analyzed by using Key-sight momentum software [50]. The antenna bandwidth is around 15% for VSWR better than 3:1. The antenna -3 dB beamwidth is 100° . The antenna gain

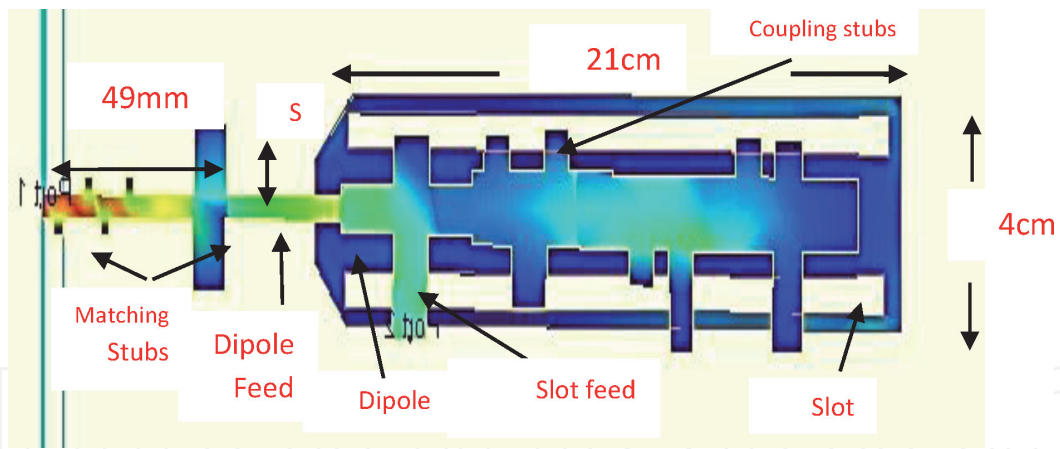


Figure 5. Current distribution of the dual-polarized wearable antenna.

is around 2 dBi. The simulated S_{11} and S_{22} parameters are shown in **Figure 6**. **Figure 7** presents the antenna's measured S_{11} parameters. The simulated radiation patterns are shown in **Figure 8**. There is a good agreement between the measured and computed results. The co-polar radiation is in the yz plane. The cross-polar radiation is in the xz plane. The antenna cross-polarization value may be adjusted by varying the feed lines and matching stubs' locations. The dimensions and current distribution of the folded antenna are shown in **Figure 9**. The radiating element

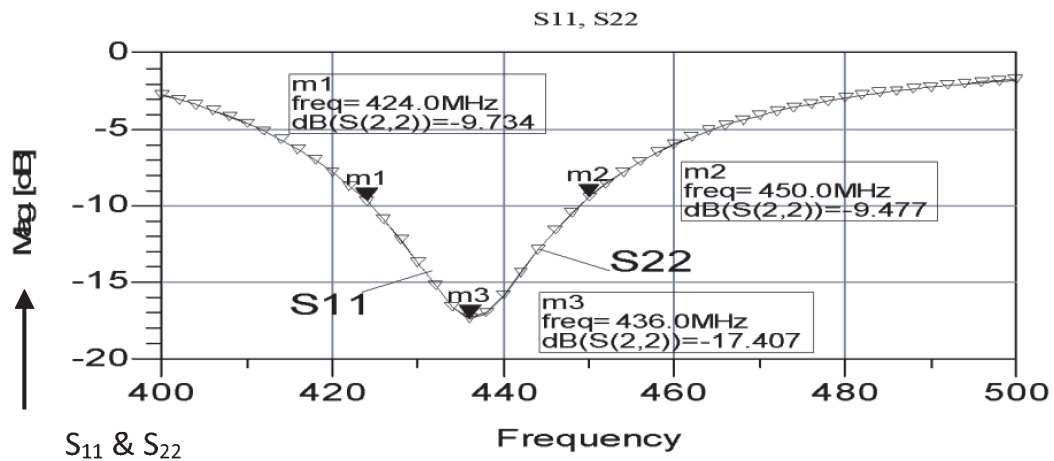


Figure 6. Computed S_{11} and S_{22} results of the dual-polarized dipole on human body.

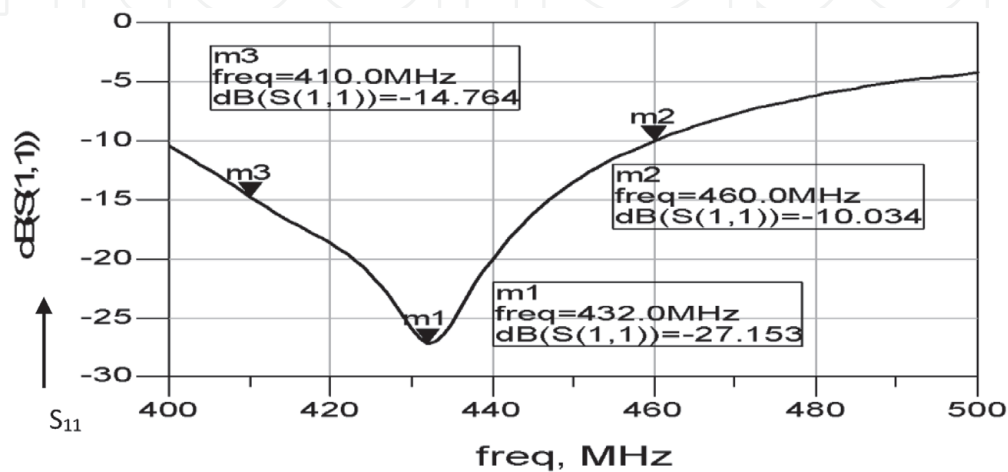


Figure 7. Measured S_{11} of the wearable dual-polarized dipole antenna on human body.

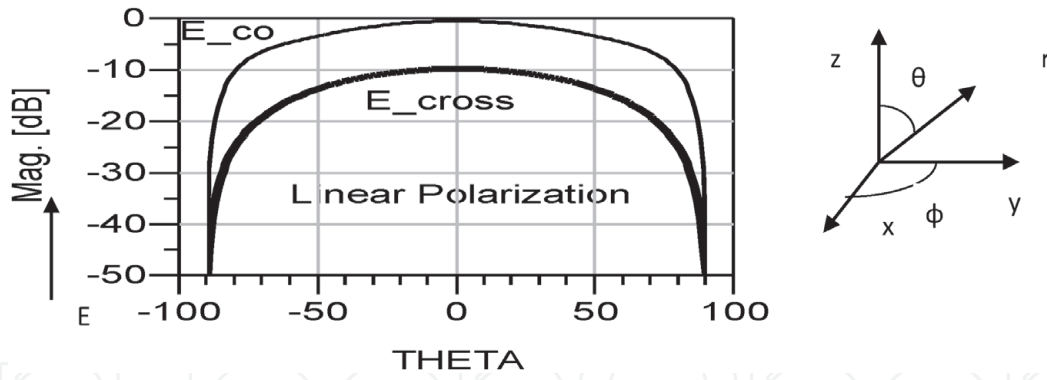


Figure 8. Radiation pattern of the dual-polarized wearable antenna.

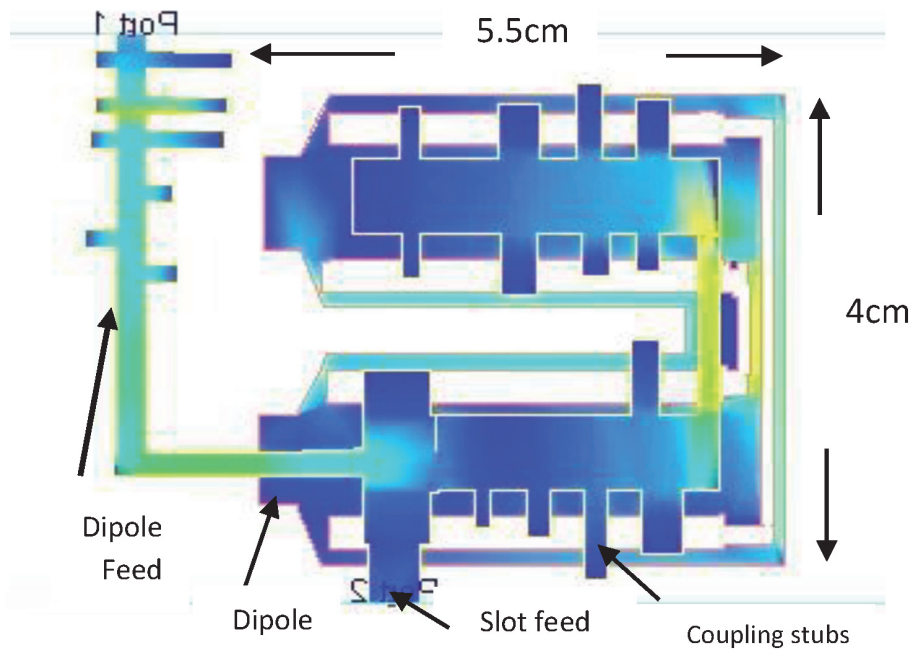


Figure 9. Current distribution of the folded wearable dipole antenna, $6 \times 5 \times 0.16$ cm.

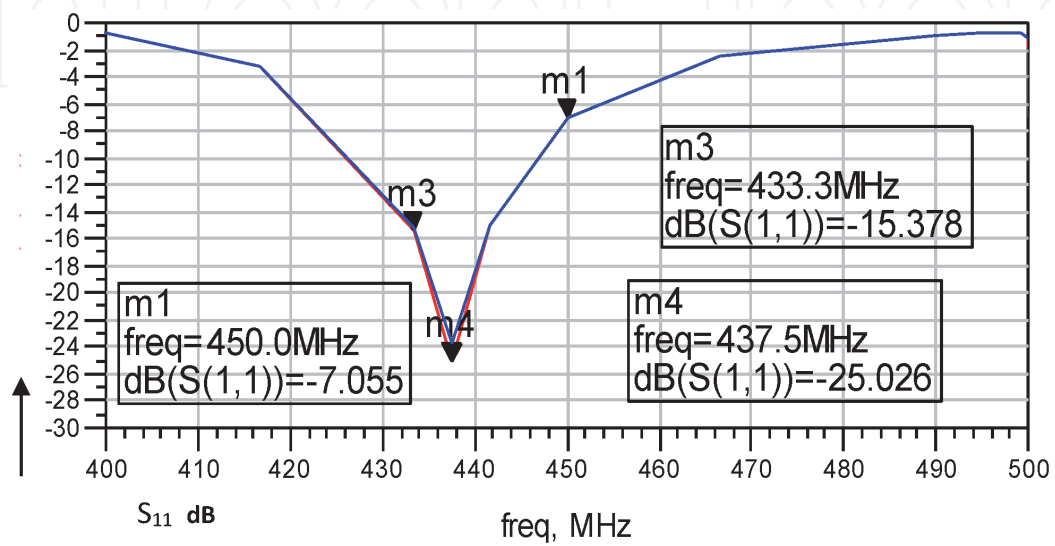


Figure 10. Folded antenna's computed S_{11} and S_{22} results on human body.

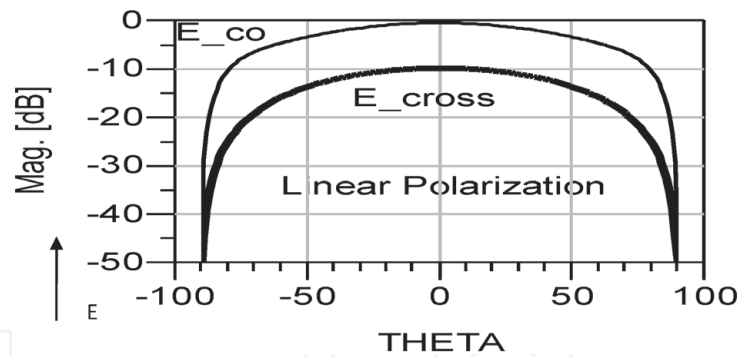


Figure 11.
 Radiation pattern of the folded dual-polarized antenna.

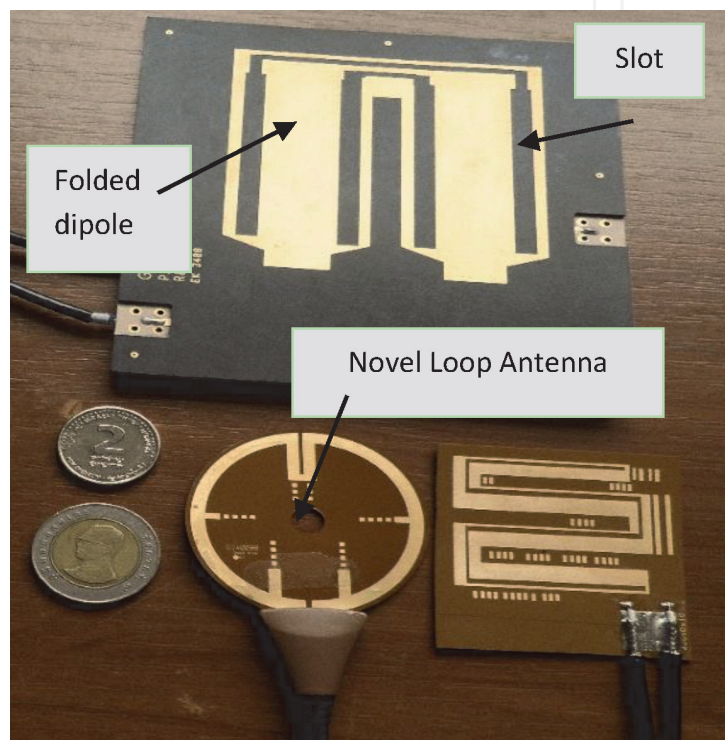


Figure 12.
 Photo of wearable antennas.

dimensions are $55 \times 40 \times 1.6$ mm. **Figure 10** presents the antenna's simulated S_{11} and S_{22} parameters. The folded dipole radiation pattern is shown in **Figure 11**. The antennas' radiation characteristics on human body were measured by using a phantom. The phantom liquid presents the body tissue's electrical characteristics. The phantom diameter is 40 cm and has 1.5 m length. The phantom liquid is a mix of 55% water, 44% sugar, and 1% salt. The wearable antenna was placed on the phantom during the measurements of the antenna's electrical characteristics. S_{11} and S_{12} parameters were measured on the patient's body by using a network analyzer. Photo of wearable antennas is shown in **Figure 12**.

4. Wearable microstrip antennas for 5G, medical, and IoT applications

Printed antennas are usually low profile, compact, flexible, light weight, and low-cost relative to wired antennas. Microstrip antennas may be used as wearable antennas. Printed antennas have been widely presented in the literature in the last 20 years, [1–19]. The most popular type of printed antennas is the microstrip

antennas. However, loop, PIFA, slot, and dipole-printed are widely used in RF systems. Printed antennas may be employed in communication mobile phones, IoT, seekers, and in medical systems.

4.1 Wearable microstrip antennas for 5G and medical systems

Microstrip antennas are etched on a low loss dielectric substrate. A cross-sectional view of the microstrip antenna electric fields is presented in **Figure 13**. Microstrip antennas are thin conducting patches etched on a substrate with dielectric constant ϵ_r and thickness H . Usually, H is less than 0.1λ . Microstrip antennas are presented in [1–7]. The wearable antenna may be attached to the human body or inserted inside a belt.

Advantages of microstrip antennas:

- Light weight and low volume.
- Flexible, Conformal structures are possible.
- Low cost relative to conventional wired antennas.
- Easy to fabricate a large uniform arrays and phased arrays.

These features are very important for wearable communication systems.

Disadvantages of microstrip antennas:

- Limited bandwidth (usually 1–5%). However, wider bandwidth is possible with increased antenna structure complexity.
- Low power handling less than 50 W depends on substrate thickness.
- Limited gain up to 30 dBi, 16×16 arrays.
- High feed network losses at high frequencies, above 12 GHz.

The patch magnetic field is perpendicular to the E-field. There is no conductor to carry the RF current so at the edge of the strip ($X/L = 0$ and $X/L = 1$), the H-field drops to zero and is maximum in the center. The E-field is zero at the center and at maximum value (and opposite polarity) at the edges ($X/L = 0$ and $X/L = 1$), see **Figure 14**. The ratio of E- to H-field is proportional to the patch impedance. Microstrip antennas may be fed by a coaxial probe feed or by a microstrip feed line.

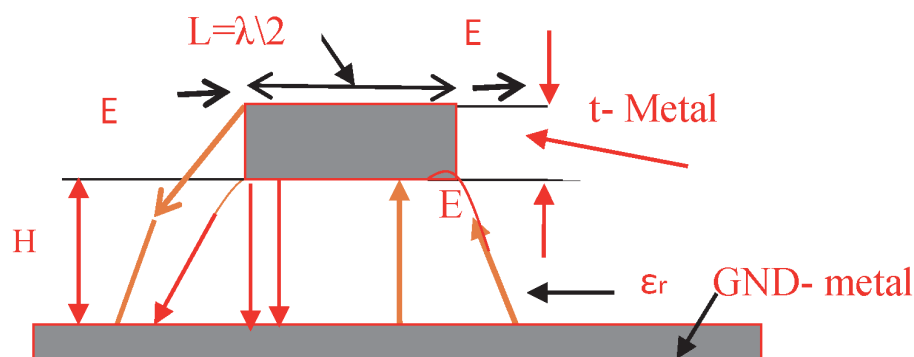


Figure 13.
Microstrip antenna electric fields, a cross-sectional view.

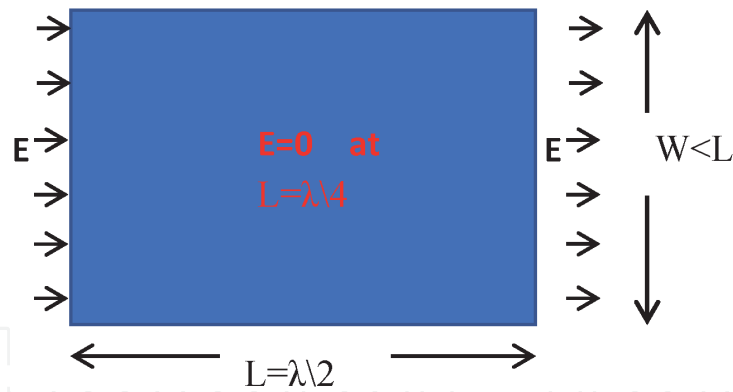
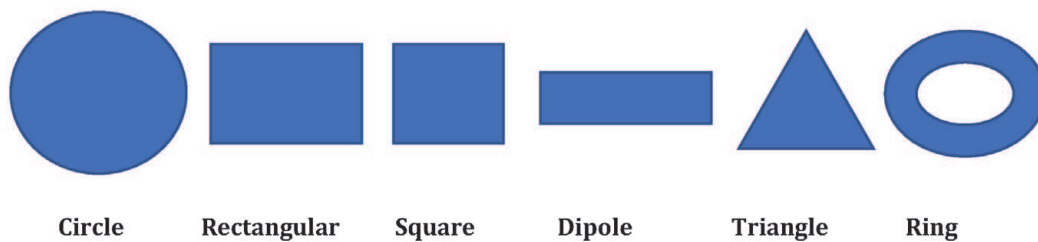


Figure 14.
 Fields of rectangular microstrip antenna.



Circle Rectangular Square Dipole Triangle Ring

Figure 15.
 Microstrip antenna popular configurations.

By adjusting the location of the antenna feed point, we can achieve any impedance and match the antenna to the RF system, usually 50 Ω. The antenna shape may be rectangular, square, triangle, circle, or any arbitrary shape as presented in **Figure 15**.

The antenna dimension, W , is given by Eq. (1) and is a function of the effective dielectric constant and resonant frequency:

$$W = \frac{c}{2f \sqrt{\epsilon_{eff}}} \quad (1)$$

The antenna bandwidth is given in Eq. (2):

$$BW = \frac{H}{\sqrt{\epsilon_{eff}}} \quad (2)$$

The gain of patch antenna is the function of the antenna effective area and can be between 0 and 5 dBi. We may increase printed antenna gain by using antenna array configuration. In low-cost microstrip antenna arrays, the RF feed network may be integrated to the radiating elements on the same substrate. Microstrip arrays feed networks are shown in **Figure 16**. A parallel feed network is illustrated in **Figure 16(a)**. A parallel series feed network is illustrated in **Figure 16(b)**.

4.2 Transmission line model of patch antennas

In the transmission line model (TLM), the patch antenna functions as two narrow slots connected by a microstrip line, as illustrated in **Figure 17**. TLM model provides a good physical understanding of the electrical characteristics of patch antennas. The electric field along and underneath the patch is given in Eq. (3) and is a function of z . In the design of a wearable patch antenna, the body electrical parameter should be considered to achieve an accurate design.

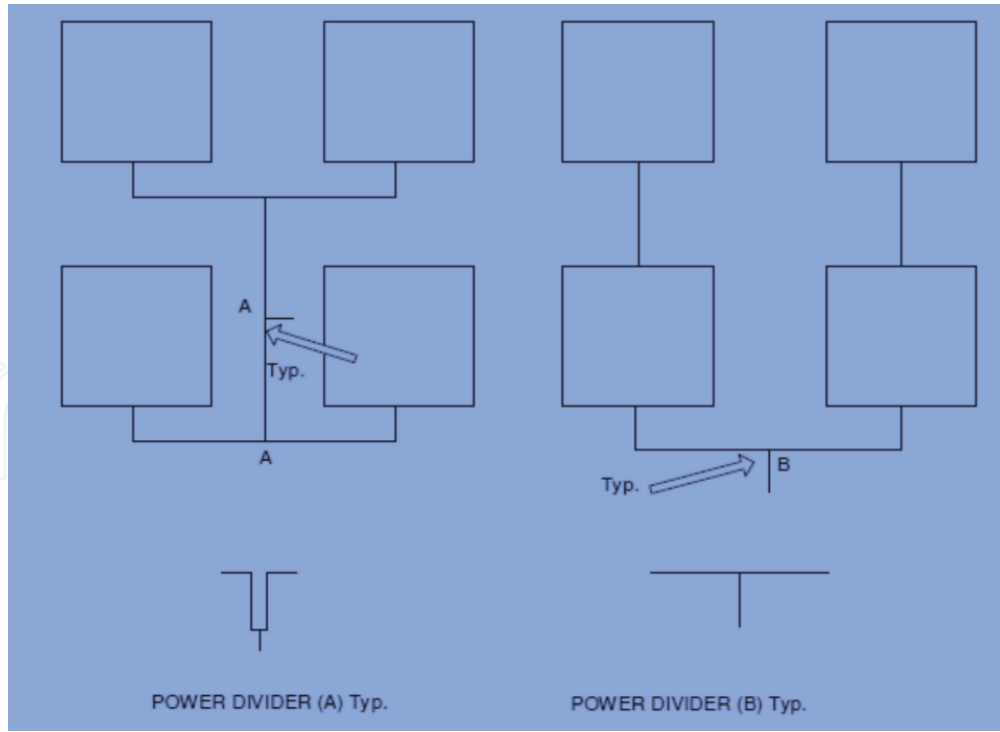


Figure 16. Configuration of integrated microstrip array and feed network. (a) Parallel feed network. (b) Parallel series feed network.

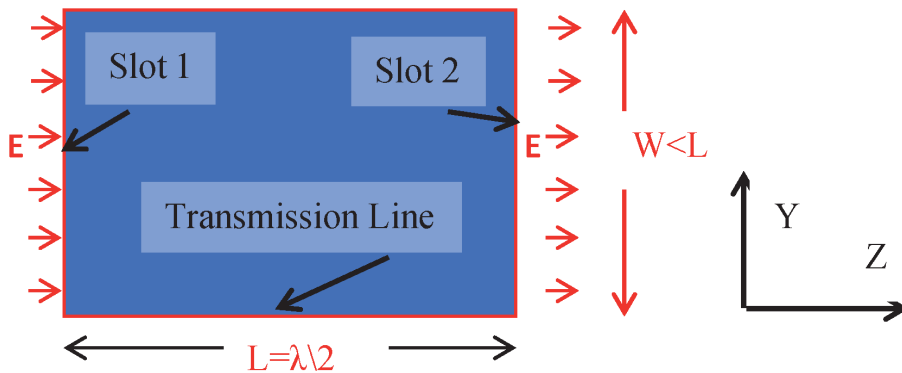


Figure 17. Patch transmission line model, two slots connected by a microstrip line.

$$E_x \sim \cos\left(\frac{\pi z}{L_{eff}}\right) \quad (3)$$

At the patch edges $z = 0$ and $z = L_{eff}$, the electric field is maximum. At the patch center $z = \frac{L_{eff}}{2}$, the electric field is equal to zero. For $\frac{H}{\lambda_0} < 0.1$, the electric field distribution along the x-axis is uniform. The slot admittance is given in Eqs. (4) and (5):

$$G = \frac{W}{120\lambda_0} \left[1 - \frac{1}{24} \left(\frac{2\pi H}{\lambda_0} \right)^2 \right] \text{ for } \frac{H}{\lambda_0} < 0.1 \quad (4)$$

$$B = \frac{W}{120\lambda_0} \left[1 - 0.636 \ln \left(\frac{2\pi H}{\lambda_0} \right)^2 \right] \text{ for } \frac{H}{\lambda_0} < 0.1 \quad (5)$$

Here, R represents the radiation losses; $G = 1/R$; and B represents the capacitive nature of the slot. At resonance, for any position of the feed point along the patch, the susceptances of both slots cancel out at the feed point. However, the patch

admittance is a function of the feed point position along the z-axis as given in Eq. (6). At the feed point, the slot admittance is transformed by the equivalent length of the transmission line. The width, W , of the microstrip antenna controls the input impedance. For a square patch antenna fed by a microstrip line, the input impedance is around 300 Ohms. By increasing the width, the impedance can be reduced. Larger widths can increase the patch bandwidth.

$$Y(l_1) = Z_0 \frac{1 + j \frac{Z_L}{Z_0} \tan \beta l_1}{\frac{Z_L}{Z_0} + j \tan \beta l_1} = Y_1 \quad (6)$$

$$Y_{in} = Y_1 + Y_2$$

4.3 Excitation of higher order modes in microstrip antennas

To prevent excitation of higher-order modes, the thickness of the substrate should be less than a tenth of the wavelength. We can calculate the cutoff frequency of the higher-order mode by using Eq. (7):

$$f_c = \frac{c}{4H\sqrt{\epsilon - 1}} \quad (7)$$

4.4 Microstrip effective dielectric constant

As shown in **Figures 13** and **14**, the edges of microstrip line and antenna part of the fields propagate in air and the other part of the fields propagates in the dielectric substrate. The effective dielectric constant is usually higher than $\frac{\epsilon_r + 1}{2}$ and is less than the substrate's dielectric constant. The effective dielectric constant of the microstrip line may be calculated by using Eqs. (8) and (9) as function of W/H :

For $\left(\frac{W}{H}\right) < 1$,

$$\epsilon_e = \frac{\epsilon_r + 1}{2} + \frac{\epsilon_r - 1}{2} \left[\left(1 + 12 \left(\frac{H}{W} \right) \right)^{-0.5} + 0.04 \left(1 - \left(\frac{W}{H} \right) \right)^2 \right] \quad (8)$$

For $\left(\frac{W}{H}\right) \geq 1$,

$$\epsilon_e = \frac{\epsilon_r + 1}{2} + \frac{\epsilon_r - 1}{2} \left[\left(1 + 12 \left(\frac{H}{W} \right) \right)^{-0.5} \right] \quad (9)$$

This calculation ignores the strip thickness and frequency dispersion. If the substrate thickness is less than tenth of a wavelength their effects are negligible.

4.5 Losses in microstrip antennas

A major part of losses in microstrip line are due to conductor loss. Radiation loss and dielectric losses are lower. Losses in microstrip lines and antennas are the major disadvantage of microstrip antennas and limit the gain and efficiency of microstrip antennas at high frequencies. Losses in microstrip lines and antennas increase significantly at high frequencies as presented in Eqs. (10) and (11).

4.5.1 Conductor loss

Conductor loss may be calculated by using Eq. (10):

$$\alpha_c = 8.686 \log (R_S / (2WZ_0)) \text{ dB/Length} \quad (10)$$

$$R_S = \sqrt{\pi f \mu \rho} \quad \text{Skin Resistance}$$

Conductor losses can be calculated by defining an equivalent loss tangent δ_c , given by $\delta_c = \delta_s/h$, and $\delta_s = \sqrt{2/\omega\mu\sigma}$. The strip conductivity is σ , μ is the free space permeability, and h is the substrate height.

4.5.2 Dielectric loss

The dielectric loss is given in Eq. (11):

$$\alpha_d = 27.3 \frac{\epsilon_r}{\sqrt{\epsilon_{eff}}} \frac{\epsilon_{eff} - 1}{\epsilon_r - 1} \frac{tg\delta}{\lambda_0} \text{ dB/cm} \quad (11)$$

$tg\delta = \text{dielectric loss coefficient}$

Losses in microstrip lines are presented in **Tables 1** and **2**. For example, total loss of a microstrip line presented in **Table 1** at 40 GHz is 0.5 dB/cm. For example, total loss of a microstrip line presented in **Table 2** at 40 GHz is 1.4 dB/cm. We may conclude that losses in microstrip lines limit the applications of microstrip technology at high frequencies.

Frequency (GHz)	Loss tangent loss (dB/cm)	Metal loss (dB/cm)	Total loss (dB/cm)
10	-0.004	-0.23	-0.23
20	-0.009	-0.333	-0.34
30	-0.013	-0.415	-0.43
40	-0.018	-0.483	-0.5

* $W = 0.12 \text{ mm}$, $Tan\delta = 0.0002$, 3 um gold , and $conductivity = 3.5E7 \text{ mhos/meter}$.

Table 1.
Microstrip line losses for a substrate of 0.127 mm thickness with $\epsilon_r = 9.9$.*

Frequency (GHz)	Tangent loss (dB/cm)	Metal loss (dB/cm)	Total loss (dB/cm)
10	-0.010	-0.66	-0.67
20	-0.02	-0.96	-0.98
30	-0.03	-1.19	-1.22
40	-0.04	-1.38	-1.42

* $W = 0.034 \text{ mm}$, $Tan\delta = 0.0004$, 3 um gold , and $conductivity = 3.5E7 \text{ mhos/meter}$.

Table 2.
Microstrip line losses for a GaAs substrate of 0.05 mm thickness with $\epsilon_r = 12.88$.*

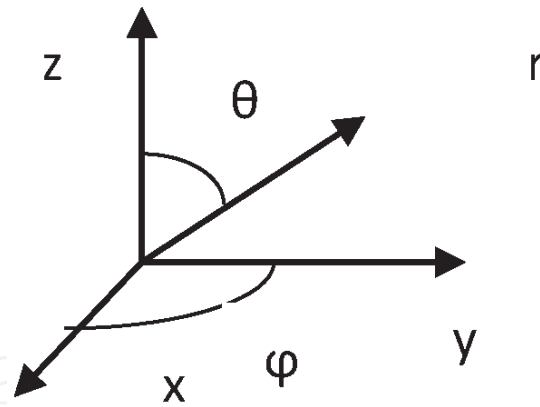


Figure 18.
 Cartesian coordinate system.

4.6 Patch radiation pattern

The patch radiation pattern is function of the patch width, W . The coordinate system is presented in **Figure 18**. The normalized radiation pattern may be simulated by using Eqs. (12) and (13):

$$E_{\theta} = \frac{\sin\left(\frac{k_0 W}{2} \sin \theta \sin \varphi\right)}{\frac{k_0 W}{2} \sin \theta \sin \varphi} \cos\left(\frac{k_0 L}{2} \sin \theta \cos \varphi\right) \cos \varphi \quad (4.11) \quad (12)$$

$$k_0 = 2\pi/\lambda$$

$$E_{\varphi} = \frac{\sin\left(\frac{k_0 W}{2} \sin \theta \sin \varphi\right)}{\frac{k_0 W}{2} \sin \theta \sin \varphi} \cos\left(\frac{k_0 L}{2} \sin \theta \cos \varphi\right) \cos \theta \sin \varphi \quad (4.12) \quad (13)$$

$$k_0 = 2\pi/\lambda$$

The magnitude of the fields is given by Eq. (14):

$$f(\theta, \varphi) = \sqrt{E_{\theta}^2 + E_{\varphi}^2} \quad (14)$$

5. Wearable stacked microstrip antennas for 5G, IoT, and medical applications

Stacked patch antennas were presented first in [1–7]. Single-layer microstrip antennas have a narrow bandwidth. This disadvantage limits the applications of microstrip antennas. By designing a double-layer microstrip antenna, we may get a wider bandwidth. Two-layer patch antennas may be the best antenna choice for wideband communication systems. On the first layer, the antenna matching network and a resonator are printed. On the second layer, the radiating element is printed. The electromagnetic field is coupled from the resonator to the radiating element. The resonator and the radiating element shapes may be rectangular, square, triangle, circle, or any other shape. The distance between the layers is optimized to get maximum bandwidth with the best antenna efficiency. The spacing between the layers may be foam or a substrate with low dielectric losses. All the antennas' electrical parameters were calculated and optimized by.

using electromagnetic software. A 2.2 GHz square patch with circular polarization stacked antenna was designed. The resonator and the feed network were printed on a substrate with a relative dielectric constant of 2.4 and with a thickness of 0.16 cm. The dimensions of the square resonator are $W = L = 4.5$ cm. The radiating element was printed on a substrate with a relative dielectric constant of 2.2 and with a thickness of 0.16 cm. The radiator is a square patch with dimensions $W = L = 4.8$ cm. The antenna is circular polarized. A 3 dB, 90° branch coupler is connected to the antenna feed lines, as shown in **Figure 19**. The antenna bandwidth is 13% for VSWR better than 3:1. The measured antenna beamwidth is 73° . The measured antenna gain is 7.5 dBi at 2.2 GHz. This antenna may be used in wideband communication systems. Comparison of calculated and measured results of stacked patch antennas is listed in **Table 3**. The antennas listed in **Table 3** may be used in wearable communication systems. Results in **Table 3** indicate that the bandwidth of stacked patch antennas may be around 9–15% for VSWR better than 2:1. There is a good agreement between the measured and calculated results. In **Figure 20**, a stacked microstrip antenna is shown. The antenna feed and matching network is printed on FR4 with a dielectric constant of 4.2 and 1.6 mm thickness. The radiator is printed on a dielectric substrate with a dielectric constant of 2.2 and 1.6 mm thickness. The dimensions of the microstrip stacked patch antenna shown in **Figure 20** are $3.3 \times 2 \times 0.32$ cm. The computed S11 parameters are presented in **Figure 21**. Radiation pattern of the microstrip stacked patch is shown in **Figure 22**.

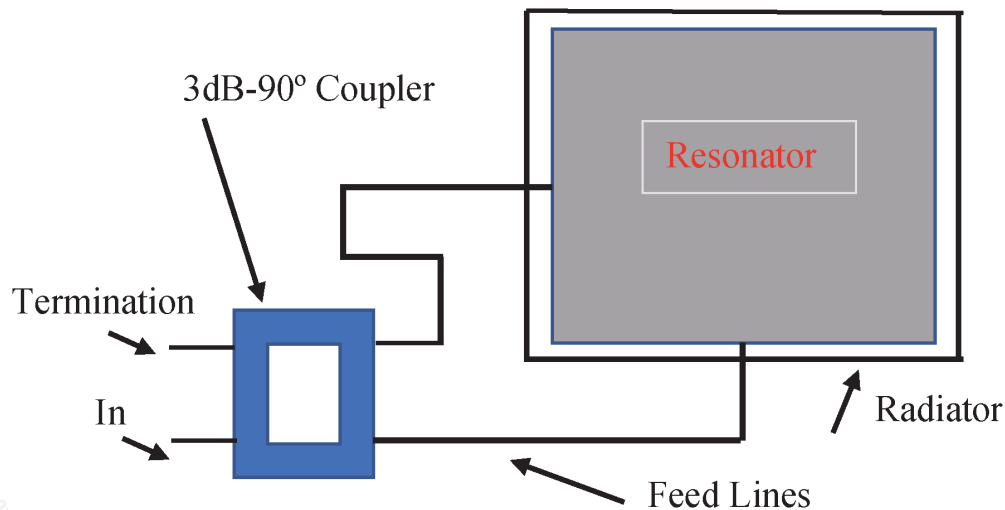


Figure 19. Feed network of a circular polarized stacked patch antenna.

Antenna	F (GHz)	Bandwidth (%)		Beamwidth		Gain (dBi)		Polarization
		Calc.	Meas.	Calc.	Meas.	Calc.	Meas.	
Square	2.2	11	10	74	72	7.5	7.5	Circular
Circular	2.2	14	15	74	72	7.5	7.9	Linear
Annular disc	2.2	12	11.5	80	78	6.5	6.6	Linear
Rectangular	2.0	10	9	72	72	7.5	7.4	Linear
Circular	2.4	10	9	74	72	7.5	7	Linear
Circular	2.4	10	10	74	72	7.5	7.5	Circular

Table 3. Comparison of calculated and measured results of stacked microstrip antennas.

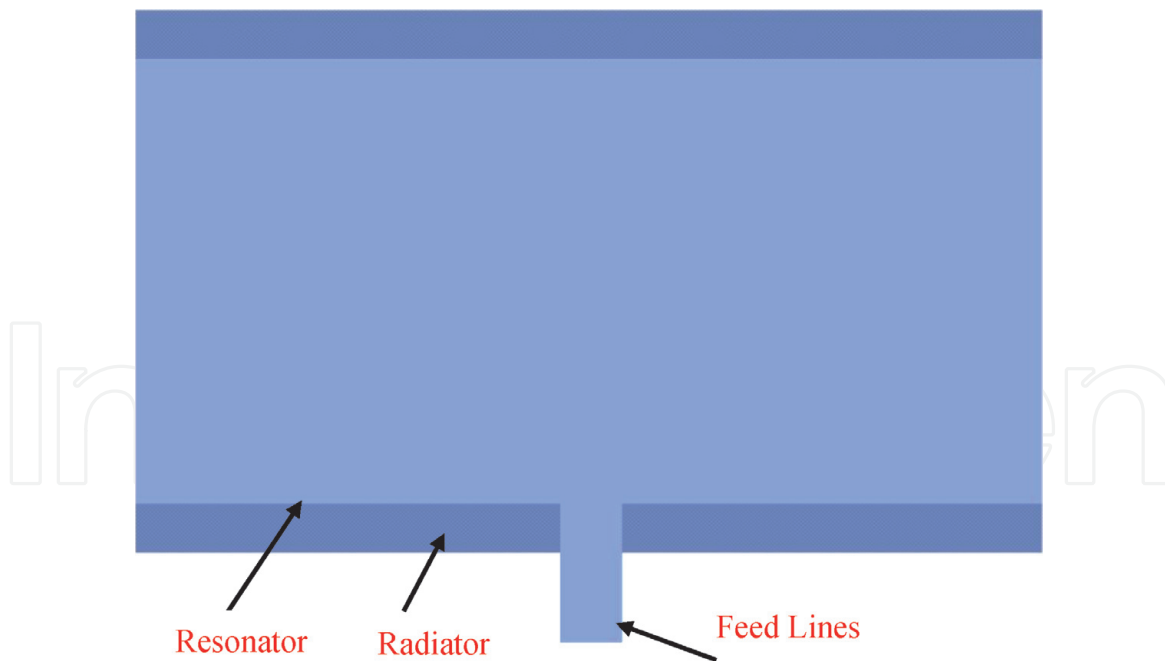


Figure 20.
A microstrip stacked patch antenna for 5G, IoT, and medical applications.

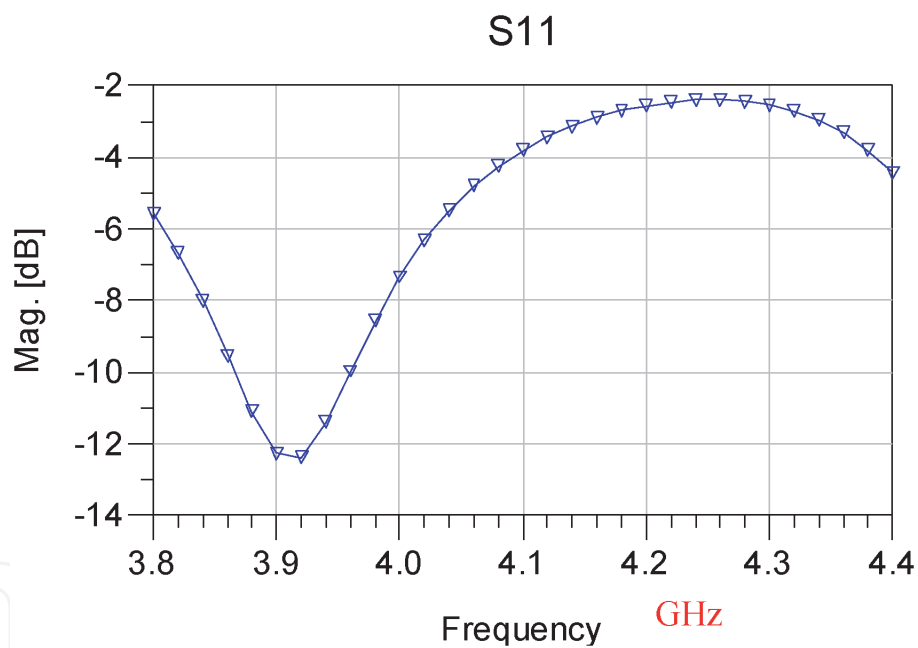


Figure 21.
Computed S11 of the microstrip stacked patch.

The antenna bandwidth is around 7% for VSWR better than 3:1. The antenna bandwidth is improved to 10% for VSWR better than 2.0:1 by adding 8 mm air spacing between the layers. The antenna beamwidth is around 72°.

The antenna gain is around 7 dBi.

5.1 Stacked microstrip 35 GHz antennas arrays

Two Ka-band, stacked patch microstrip antenna arrays, which consist of 256 radiating elements, have been designed on a substrate with $\epsilon_r = 2.2$, 0.25 mm thick. The first Type A array with a parallel feed network, is shown in **Figure 16(a)**. The second Type B array is shown in **Figure 16(b)** has more bend discontinuities in the

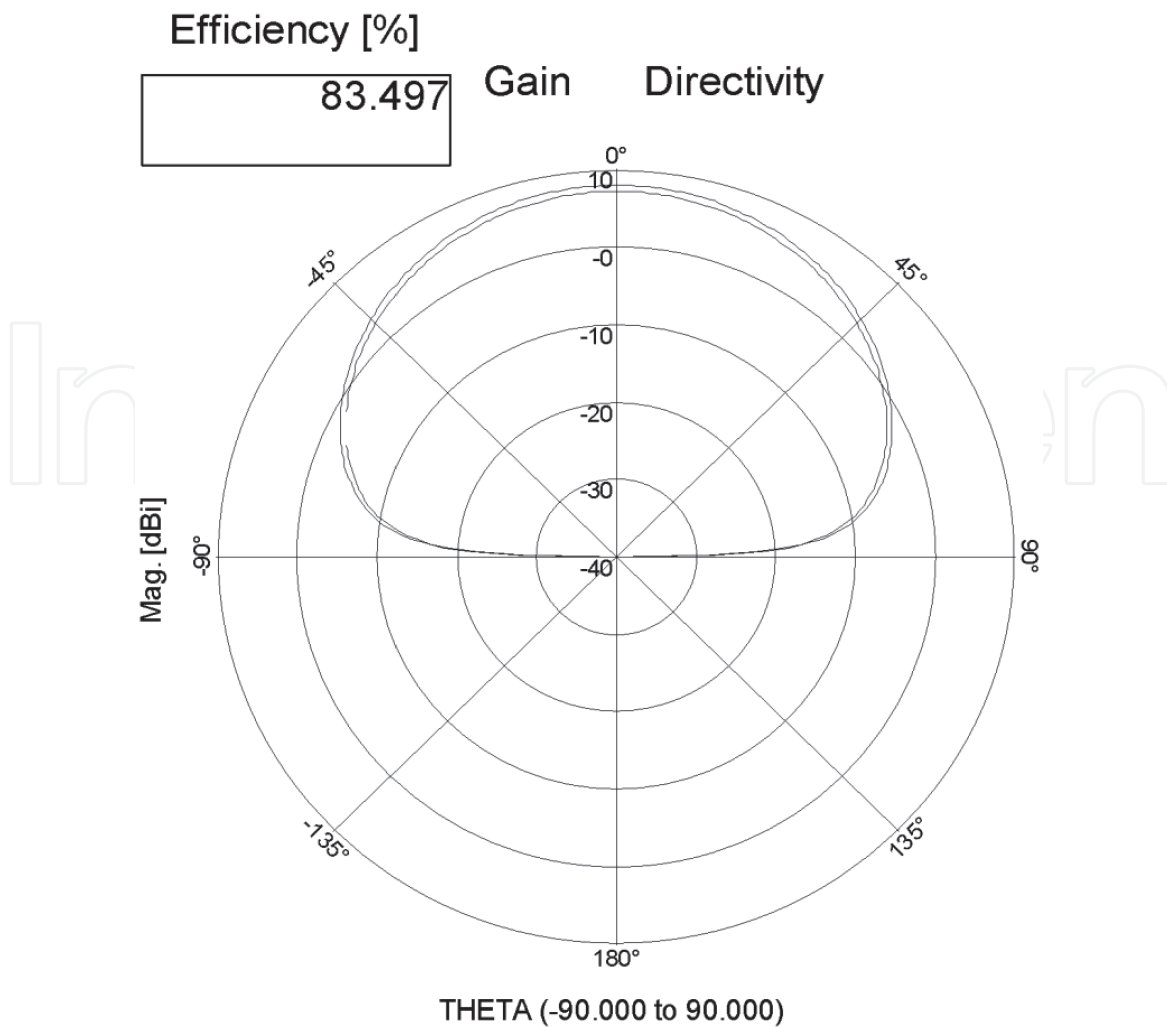


Figure 22.
Radiation pattern of the microstrip stacked patch.

Parameter	Type A	Type B	Type C
Number of radiators	256	256	256
Beamwidth (°)	4.2	4.2	4.2
Computed gain(dBi)	32	32	32
Microstrip line loss(dB)	3.1	3.1	1.5
Radiation loss T-J. (dB)	0.72	0.72	0.72
Radiation loss bends(dB)	0.13	1.17	0.13
Radiation loss steps(dB)	0.12	—	0.12
Mismatch Loss (dB)	0.5	0.5	0.5
Expected Gain(dBi)	27.43	26.5	29.03
Measured Gain(dBi)	27.5	26.5	29.5
Efficiency (%)	34.9	28.2	51

Table 4.
Comparison of electrical performance of 256 stacked patch microstrip antenna arrays.

feeding network than Type A array. In the Type C array, a 10-cm coaxial line was used to replace the same length of microstrip line in the Type A array. Comparison of measured results of the arrays, given in **Table 4**, shows that the gain of the

modified array Type C was increased by 1.6 dB. The arrays' measured bandwidth is around 12% for VSWR better than 2:1.

6. Stacked mono-pulse Ku-band patch antenna

A mono-pulse double-layer circular patch antenna was designed at Ku band, 15 GHz. The mono-pulse antenna consists of four circular patch antennas and a feed network as presented in **Figure 23**. The circular resonator and the branch coupler were printed on a substrate with a relative dielectric constant of 2.45 and with a thickness of 0.8 mm. The diameter of the circular microstrip resonator is 0.42 cm. The circular radiator was printed on a substrate with a relative dielectric constant of 2.25 and with a thickness of 0.8 mm. The diameter of the circular patch is 0.45 cm. The comparator consists of three 3 dB, 180° rat-race couplers that are connected to four circular patches via the antenna feed lines, as presented in **Figures 23** and **24**. The strip-line 3 dB, 180° rat-race couplers are printed on a substrate with a relative dielectric constant of 2.2 and thickness of 0.8 mm. The comparator structure and ports are shown in **Figures 23** and **24**. The comparator output ports are: a sum port Σ , difference port Δ , an azimuth difference port ΔAz , and an elevation difference port ΔEl . The antenna bandwidth is 11% for VSWR better than 2:1. The antenna beam width is around 36°. The computed and measured antenna gain is around 10.5 dBi. The maximum comparator losses are 0.75 dB.

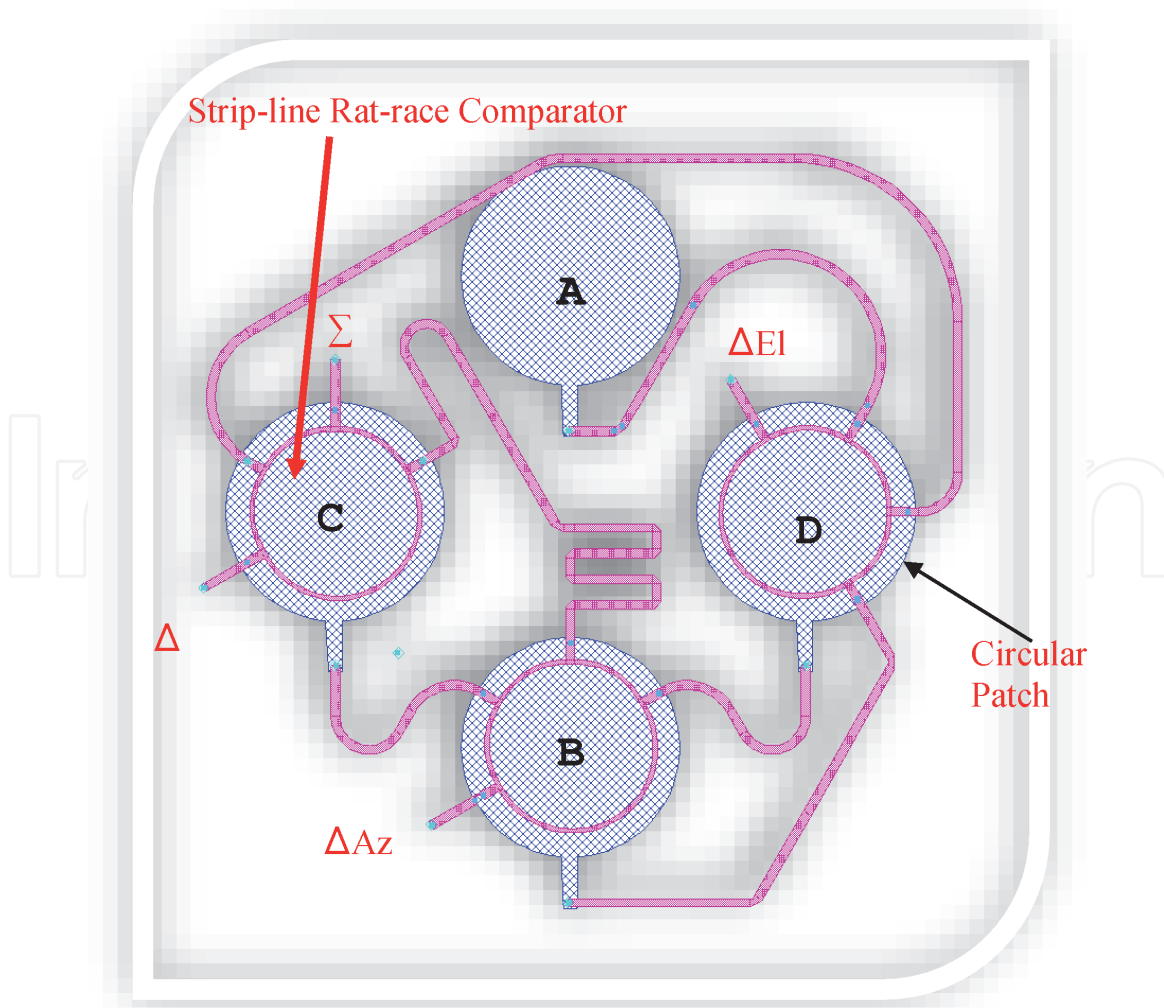


Figure 23.
A microstrip stacked mono-pulse antenna.

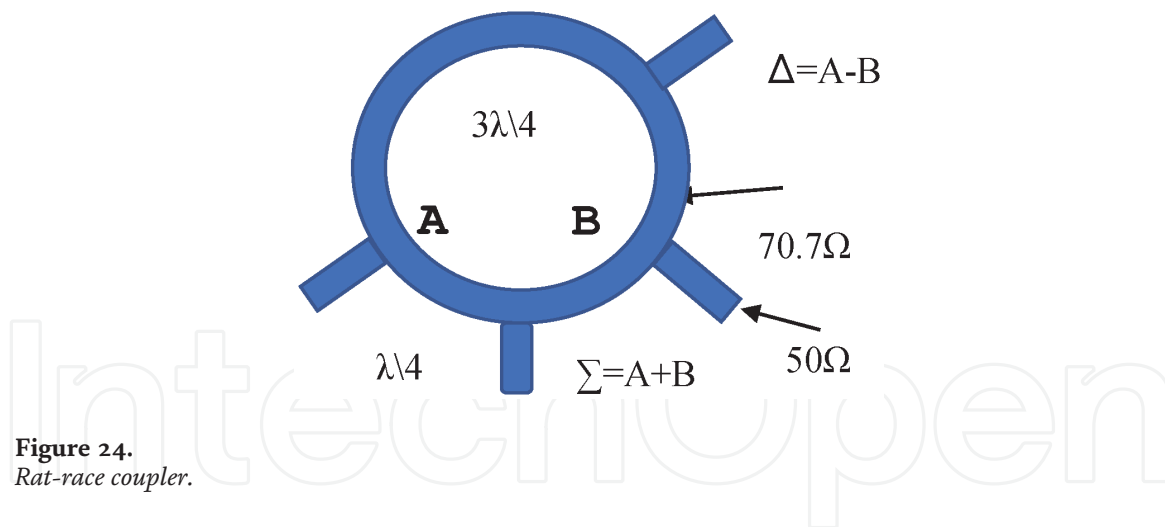


Figure 24.
Rat-race coupler.

6.1 Rat-race coupler

A rat-race coupler is shown in **Figure 24**. The rat-race circumference is 1.5 wavelengths. The distance from A to Δ port is $3\lambda/4$. The distance from A to Σ port is $\lambda/4$.

For an equal-split rat-race coupler, the impedance of the entire ring is fixed at $1.41 \times Z_0$, or 70.7Ω for $Z_0 = 50\Omega$. For an input signal V , the outputs at ports 2 and 4 are equal in magnitude, but 180 degrees out of phase.

7. Wearable Metamaterial antennas for 5G, IoT, and medical applications

Low profile efficient antennas are crucial in the development of commercial compact 5G communication and IoT systems. Communication, IoT, and biomedical industries are in rapid growth in the last years. It is important to develop efficient high gain compact antennas for 5G communication and IoT systems. Metamaterials and fractal structures may be used to improve the efficiency of compact printed antennas. In this chapter metamaterial antennas will be presented.

7.1 Introduction

Small printed antennas suffer from low efficiency. Metamaterial technology is used to design wearable compact antennas with high efficiency. The metamaterial antennas may be used in 5G communication systems, IoT, and medical systems. Design trade-offs, development, and computed and measured results of compact, efficient metamaterial antennas are presented in this chapter. The gain and directivity of the patch antenna with split ring resonators (SRRs) are higher by 2.5 dB than the patch antenna without SRR. The resonant frequency of the antenna with SRR on human body is shifted by 3%. Printed antennas are used in communication systems and are presented in journals and books, as referred in [1–5]. Microstrip and printed antennas have several advantages such as being light weight, compact, flexible, and having low production cost. The main disadvantages of these printed antennas are narrow bandwidth and low efficiency. In Ref. [51], artificial media with negative dielectric permittivity were presented. Materials with dielectric constant and permeability less than 1 are developed by using periodic SRR and metallic posts structures as presented in [51–59]. New wearable printed metamaterial antennas with high efficiency are presented in this chapter.

7.2 Stacked microstrip antenna with SRR

Stacked microstrip patches antennas with and without SRR has been designed, see Refs. [1–5]. The antennas was designed on the same substrate. The antennas are stacked double-layer antennas. The first layer consists of a FR4 substrate with a dielectric constant of 4.2 and 1.6 mm thickness. The second layer consists of a dielectric substrate with a dielectric constant of 2.3 and 1.6 mm thickness. The antenna has been analyzed and optimized by using full wave electromagnetic software. The dimensions of the microstrip stacked patch antenna are $33 \times 20 \times 3.2$ mm as presented in **Figure 25**. The antenna bandwidth is around 6% for VSWR better than 3:1. The antenna beam width is around 74° . The stacked antenna directivity and gain are around 7 dBi. The computed S11 parameters are presented in **Figure 26**. Radiation pattern of the microstrip stacked patch is shown in **Figure 27**. The stacked patch antenna with SRR is presented in **Figure 28**. This antenna has the same structure as the stacked antenna shown in **Figure 25**. The spacing between the SRR rings is 0.25 mm and the ring width is 0.2 mm. Four rows of seven SRRs are placed on the radiating patch. The measured S11 parameters of the antenna with SRR are presented in **Figure 29**. The antenna bandwidth is around 13% for VSWR better than 2.5:1. By adding an air space of 4 mm between the antenna layers, the VSWR was improved to 2:1. The antenna gain is around 9–10 dBi. The antenna's

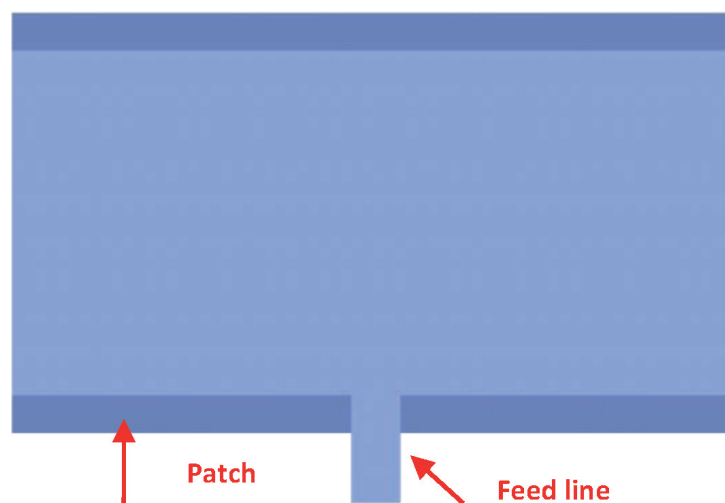


Figure 25.
A microstrip stacked patch antenna.



Figure 26.
Computed S11 of the microstrip stacked patch.

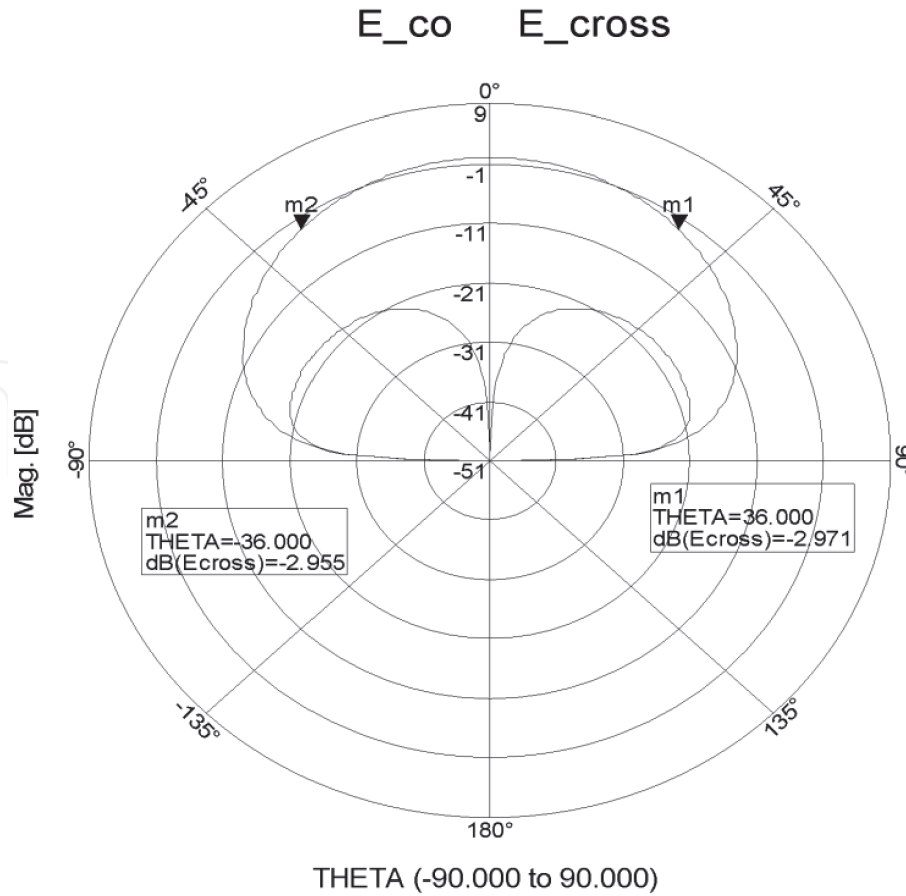


Figure 27.
Radiation pattern of the microstrip stacked patch.

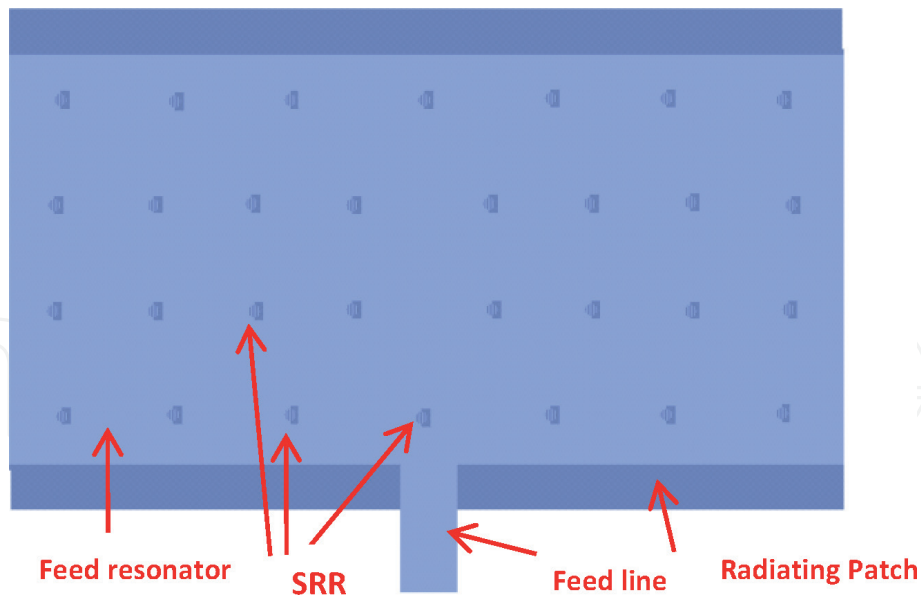


Figure 28.
Printed antenna with split ring resonators.

efficiency is around 95%. The antenna computed radiation pattern is shown in **Figure 30**. There is a good agreement between the measured and computed results. The effective area of a patch antenna without SRR is lower than the effective area of a patch antenna with SRR. The resonant frequency of a patch antenna without SRR is higher by 10% than the resonant frequency of a patch antenna with SRR. The antenna beamwidth is around 70°. The directivity and gain of the stacked antenna with SRR is higher by 2–3 dB than the patch antenna without SRR.

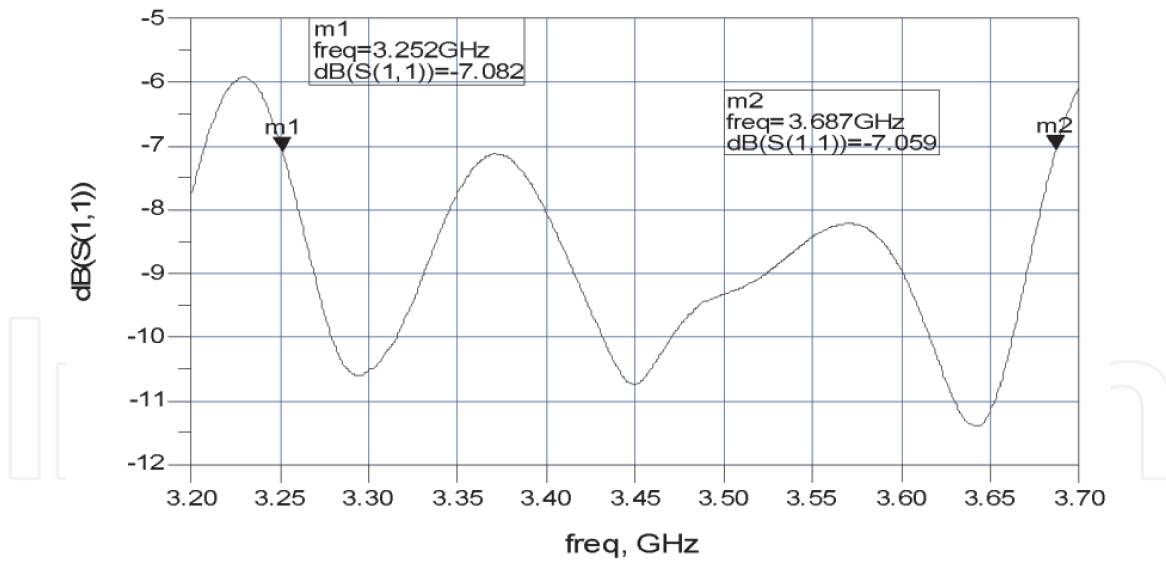


Figure 29.
 Patch with split ring resonators for medical and 5G applications, measured S_{11} .

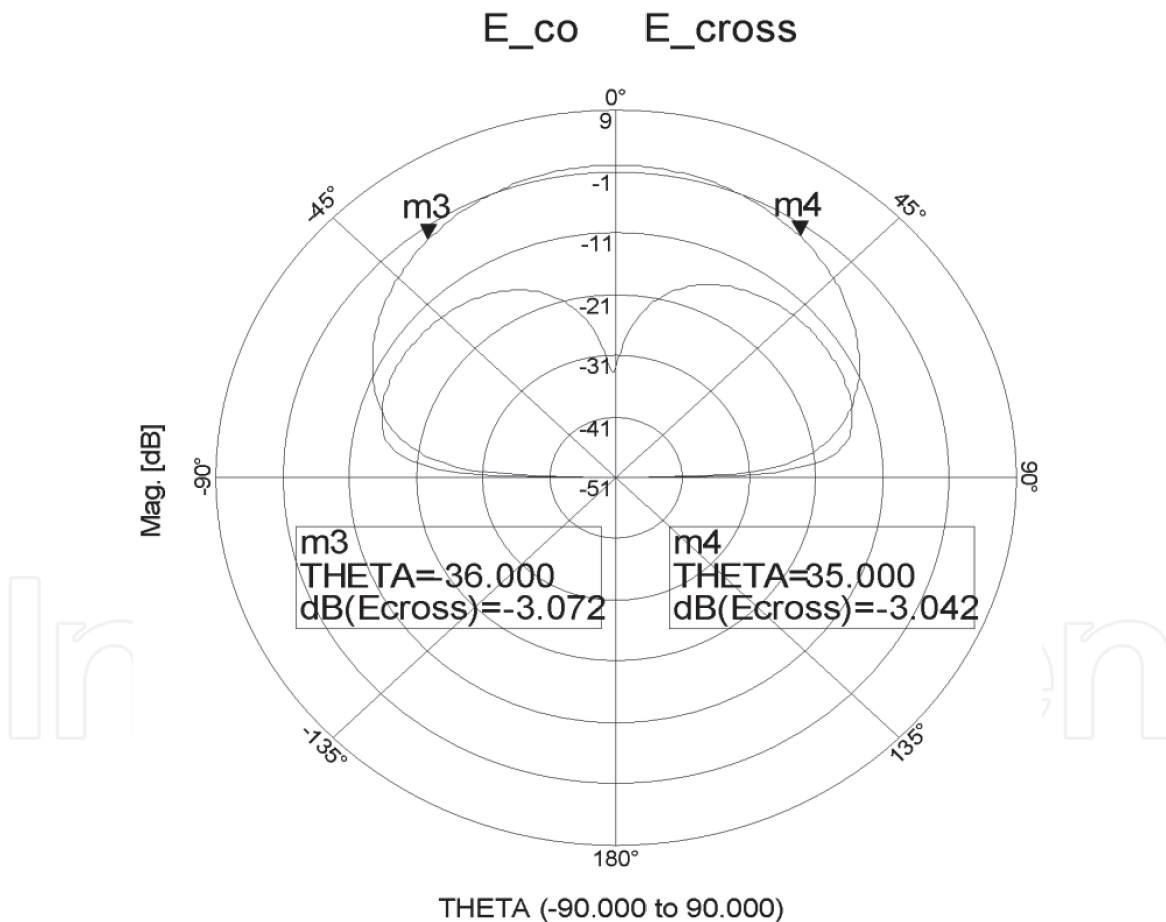


Figure 30.
 Radiation pattern for patch with SRR for medical and 5G applications.

7.3 Patch antenna with split ring resonators

A patch antenna with split ring resonators was developed. The antenna is printed on the dielectric substrate with a dielectric constant of 2.2 and with a 1.6 mm thickness. The dimensions of the microstrip patch antenna shown in

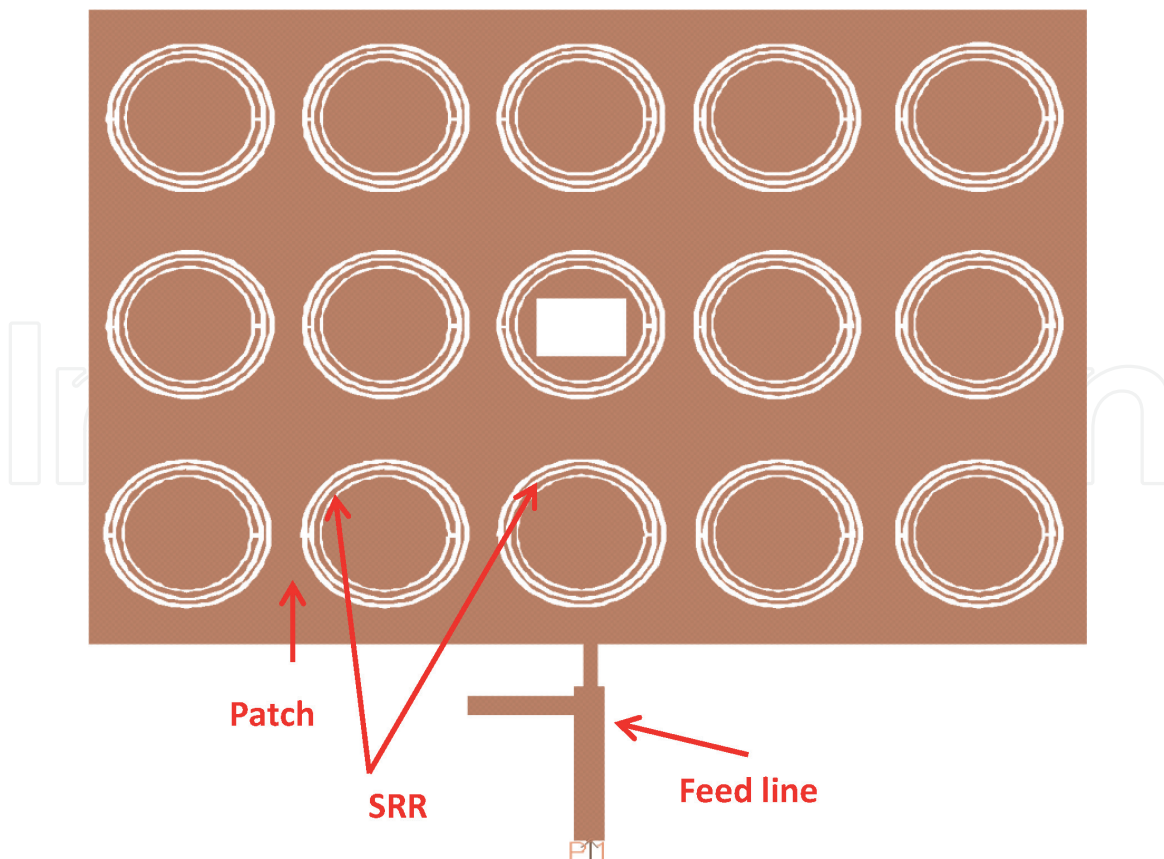


Figure 31.
Patch antenna with 15 Split ring resonators.

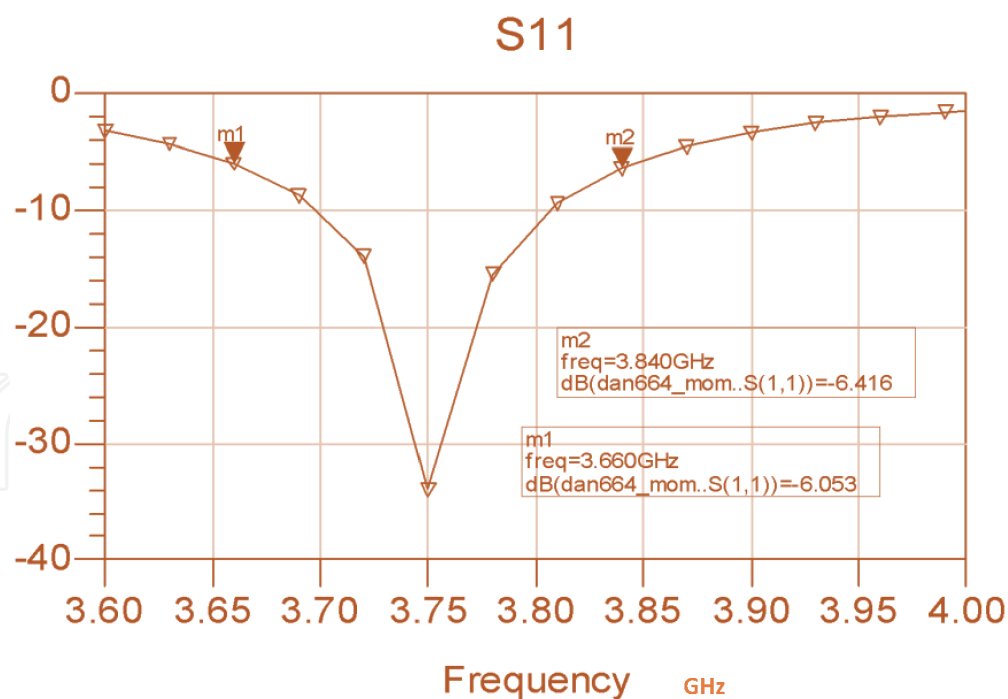


Figure 32.
Patch with 15 split ring resonators, computed S_{11} .

Figure 31 are $36 \times 20 \times 1.6$ mm. The metamaterial antenna bandwidth is around 6% for VSWR better than 2:1. The antenna bandwidth is around 9% for S_{11} lower than -6 dB. The antenna directivity and gain are around 7.5 dBi. The computed and measured antenna beam width is around 72° . The antenna efficiency is 77.25%. The measured S_{11} parameters are presented in **Figure 32**. The gain and directivity of the

patch antenna with SRR is higher by 2.5 dB than the patch antenna without SRR. A photo of printed metamaterial antennas for medical and IoT applications is shown in **Figure 33**. Metamaterial patch antenna with SRR for 5G, IoT, and medical

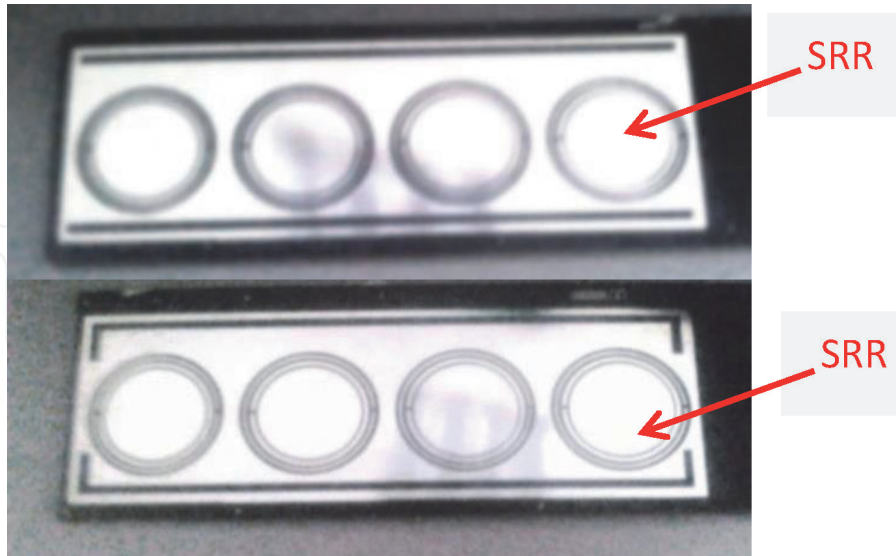


Figure 33.
Photo of printed metamaterial antennas for medical applications.

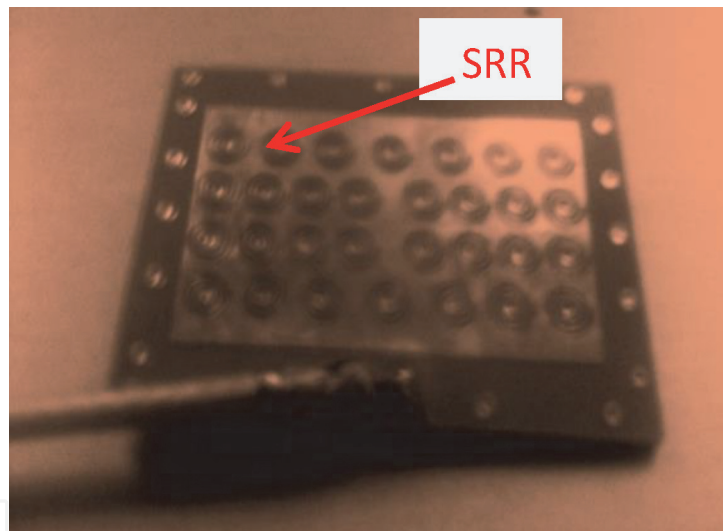


Figure 34.
Photo of metamaterial patch antenna with SRR.

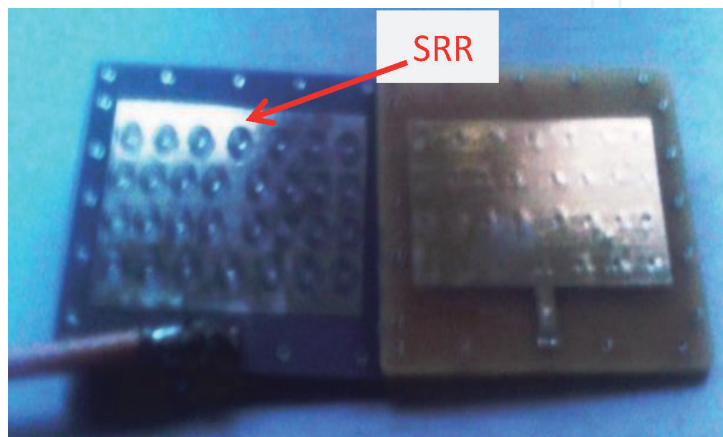


Figure 35.
Meta-material stacked patch antenna with SRR.

applications is shown in **Figure 34**. Metamaterial stacked patch antenna with SRR for 5G, IoT, and medical applications is shown in **Figure 35**.

8. Conclusions

This chapter presents several wideband wearable antennas with high efficiency for medical, IoT and sport applications. Wearable technology provides a useful novel tool to health-care centers and surgical rehabilitation services. Wireless wearable body area network (wireless WBAN) is emerging as a significant option for hospitals, medical centers, and patients. Wearable devices provide a useful network that may improve the long-term context and physiological response of patients and health-care customers. Wearable devices and technology will help to develop personal treatment devices with online and real-time feedback to improve patient's health. Wearable medical devices and sensors can measure heartbeat, blood pressure, body temperature, and sweat rate, perform gait analysis, and measure almost any medical parameters of the patient wearing the medical system.

Design considerations computed and measured results of several wearable printed antennas are described in this chapter. The antenna's electrical characteristics and dimensions were designed to meet the medical system specification. The dimensions of the compact antennas may vary from $260 \times 60 \times 1.6$ mm to $50 \times 50 \times 0.5$ mm to meet the medical system specification. The compact wearable antennas bandwidth is between 9 and 12% for VSWR better than 2:1. The compact wearable antenna beam width varies from 72° to 100° and the wearable antennas gain varies from 0 to 5 dBi as a function of the antenna dimensions.

The length of the antennas without SRR is higher by 5–10% than the length of the antennas with SRR. Moreover, the resonant frequency of the antennas without SRR is higher by 5–10% than the antennas with SRR. The gain and directivity of the patch antenna without SRR is lower by 2–3 dB than the patch antenna with SRR. The resonant frequency of the wearable antennas with SRR on human body may be shifted by 2–5%.


IntechOpen

Author details

Albert Sabban
Kinneret College, Emek Hayarden, Israel

*Address all correspondence to: sabban@netvision.net.il

IntechOpen

© 2020 The Author(s). Licensee IntechOpen. This chapter is distributed under the terms of the Creative Commons Attribution License (<http://creativecommons.org/licenses/by/3.0>), which permits unrestricted use, distribution, and reproduction in any medium, provided the original work is properly cited. 

References

- [1] Sabban A. Wideband RF Technologies and Antenna in Microwave Frequencies. USA: Wiley Sons; 2016
- [2] Sabban A. Novel Wearable Antennas for Communication and Medical Systems. FL, USA: Taylor & Francis Group; 2017
- [3] Sabban A. Low Visibility Antennas for Communication Systems. USA: Taylor & Francis Group; 2015
- [4] Sabban A. Small wearable meta materials antennas for medical systems. The Applied Computational Electromagnetics Society Journal. April 2016;31(4):434-443
- [5] Sabban A. Microstrip antenna arrays. In: Nasimuddin N, editor. Microstrip Antennas. Croatia: InTech; 2011. pp. 361-384. ISBN: 978-953-307-247-0. Available from: <http://www.intechopen.com/articles/show/title/microstrip-antenna-arrays>
- [6] Sabban A. New wideband printed antennas for medical applications. IEEE Transactions on Antennas and Propagation. 2013;61(1):84-91
- [7] Sabban A. Dual polarized dipole wearable antenna. USA: U.S Patent Number: 8203497; 2012
- [8] Sabban A. A new wideband stacked microstrip antenna. In: IEEE Antenna and Propagation Symposium. Houston, Texas, USA; June 1983
- [9] Sabban A. Wideband microstrip antenna arrays. In: IEEE Antenna and Propagation Symposium MELCOM, Tel-Aviv, June 1981. 1981
- [10] Chirwa* Lawrence C, Hammond Paul A, Scott Roy Cumming David RS. "Electromagnetic radiation from ingested sources in the human intestine between 150 MHz and 1.2 GHz", IEEE Transactions on Biomedical Engineering. April 2003;50(4):484-492
- [11] Werber D, Schwentner A, Biebl EM. Investigation of RF transmission properties of human tissues. Advances in Radio Science. 2006;4:357-360
- [12] Thalmann T, Popovic Z, Notaros BM, Mosig JR. Investigation and design of a multi-band wearable antenna. In: 3rd European Conference on Antennas and Propagation. Berlin, Germany: EuCAP 2009; 2009. pp. 462-465
- [13] Salonen P, Rahmat-Samii Y, Kivikoski M. Wearable antennas in the vicinity of human body. In: IEEE Antennas and Propagation Society Symposium, Vol. 1, Monterey USA, 2004. 2004. pp. 467-470
- [14] Fujimoto K, James JR, editors. Mobile Antenna Systems Handbook. Boston USA: Artech House; 1994
- [15] Gupta B, Sankaralingam S, Dhar S. Development of wearable and implantable antennas in the last decade. In: Microwave Mediterranean Symposium (MMS), August 2010, Guzelyurt, Turkey. 2010. pp. 251-267
- [16] Kellomaki T, Heikkinen J, Kivikoski M. Wearable antennas for FM reception. In: First European Conference on Antennas and Propagation, EuCAP 2006, Hague, the Netherlands. 2006. pp. 1-6
- [17] Sabban A. Wideband printed antennas for medical applications. In: APMC 2009 Conference, Singapore, 12/2009. 2009
- [18] Lee Y. Antenna Circuit Design for RFID Applications. Az, USA: Microchip Technology Inc., Microchip AN 710c. 2003
- [19] Sabban A, Gupta KC. Characterization of radiation loss from

microstrip discontinuities using a multiport network modeling approach. *IEEE Transactions on MTT*. 1991;39(4): 705-712

[20] Sabban A. Multiport network model for evaluating radiation loss and coupling among discontinuities in microstrip circuits [PhD thesis]. Colorado, Boulder, USA: University of Colorado at Boulder; 1991

[21] Mukhopadhyay SC, editor. *Wearable Electronics Sensors*. Switzerland: Springer; 2015

[22] Bonfiglio A, De Rossi D, editors. *Wearable Monitoring Systems*, Springer, NY, USA, 2011

[23] Gao T, Greenspan D, Welsh M, Juang RR, Alm A. Vital signs monitoring and patient tracking over a wireless network. In: *Proceedings of IEEE-EMBS 27th Annual International Conference of the Engineering in Medicine and Biology*, Shanghai, China, 1–5 September 2005. 2005. pp. 102-105

[24] Otto CA, Jovanov E, Milenkovic EA. WBAN-based system for health monitoring at home. In: *Proceedings of IEEE/EMBS International Summer School, Medical Devices and Biosensors*, Boston, MA, USA, 4–6 September 2006. 2006. pp. 20-23

[25] Zhang GH, Poon CCY, Li Y, Zhang YT. A biometric method to secure telemedicine systems. In: *Proceedings of the 31st Annual International Conference of the IEEE Engineering in Medicine and Biology Society*, Minneapolis, MN, USA, September 2009. 2009. pp. 701-704

[26] Srinivasan V, Stankovic J, Whitehouse K. Protecting your daily in home activity information from a wireless snooping attack. In: *Proceedings of the 10th International Conference on Ubiquitous Computing*,

Seoul, Korea, 21–24 September 2008. 2008. pp. 202-211

[27] Casas R, Blasco MR, Robinet A, Delgado AR, Yarza AR, McGinn J, et al. User modelling in ambient intelligence for elderly and disabled people. In: *Proceedings of the 11th International Conference on Computers Helping People with Special Needs*, Linz, Austria, July 2008. 2008. pp. 114-122

[28] Jasemian Y. Elderly comfort and compliance to modern telemedicine system at home. In: *Proceedings of the Second International Conference on Pervasive Computing Technologies for Healthcare*, Tampere, Finland, 30 January–1 February 2008. 2008. pp. 60-63

[29] Atallah L, Lo B, Yang GZ, Siegemund F. Wirelessly accessible sensor populations (WASP) for elderly care monitoring. In: *Proceedings of the Second International Conference on Pervasive Computing Technologies for Healthcare*, Tampere, Finland, 30 January–1 February 2008. 2008. pp. 2-7

[30] Hori T, Nishida Y, Suehiro T, Hirai S. SELF-network: Design and implementation of network for distributed embedded sensors. In: *Proceedings of IEEE/RSJ International Conference on Intelligent Robots and Systems*, Takamatsu, Japan, 30 October–5 November 2000. 2000. pp. 1373-1378

[31] Mori Y, Yamauchi M, Kaneko K. Design and implementation of the vital sign box for home healthcare. In: *Proceedings of IEEE EMBS International Conference on Information Technology Applications in Biomedicine*, Arlington, VA, USA, November 2000. 2000. pp. 104-109

[32] Lauterbach C, Strasser M, Jung S, Weber W. Smart clothes self-powered by body heat. In: *Proceedings of*

Avantex Symposium, Frankfurt, Germany, May 2002. 2002. pp. 5259-5263

[33] Marinkovic S, Popovici E. Network coding for efficient error recovery in wireless sensor networks for medical applications. In: Proceedings of International Conference on Emerging Network Intelligence, Sliema, Malta, 11–16 October 2009. 2009. pp. 15-20

[34] Schoellhammer T, Osterweil E, Greenstein B, Wimbrow M, Estrin D. Lightweight temporal compression of microclimate datasets. In: Proceedings of the 29th Annual IEEE International Conference on Local Computer Networks, Tampa, FL, USA, 16–18 November 2004. 2004. pp. 516-524

[35] Barth AT, Hanson MA, Powell HC Jr, Lach J. Tempo 3.1: A body area sensor network platform for continuous movement assessment. In: Proceedings of the 6th International Workshop on Wearable and Implantable Body Sensor Networks, Berkeley, CA, USA, June 2009. 2009. pp. 71-76

[36] Gietzelt M, Wolf KH, Marschollek M, Haux R. Automatic self-calibration of body worn triaxial-accelerometers for application in healthcare. In: Proceedings of the Second International Conference on Pervasive Computing Technologies for Healthcare, Tampere, Finland, January 2008. 2008. pp. 177-180

[37] Gao T, Greenspan D, Welsh M, Juang RR, Alm A. Vital signs monitoring and patient tracking over a wireless network. In: Proceedings of the 27th Annual International Conference of the IEEE EMBS, Shanghai, China, 1–4 September 2005. 2005. pp. 102-105

[38] Baker C, Armijo K, Belka S, Benhabib M, Bhargava V, Burkhart N, et al. Wireless sensor networks for home health care. In: Proceedings of the 21st International Conference on Advanced

Information Networking and Applications Workshops, Niagara Falls, Canada, 21–23 May 2007. 2007. pp. 832-837

[39] Aziz O, Lo B, King R, Darzi A, Yang GZ. Pervasive body sensor network: An approach to monitoring the postoperative surgical patient. In: Proceedings of International Workshop on Wearable and Implantable Body Sensor Networks (BSN 2006), Cambridge, MA, USA; 2006. pp. 13-18

[40] Kwon DY, Gross M. Combining body sensors and visual sensors for motion training. In: Proceedings of the 2005 ACM SIGCHI International Conference on Advances in Computer Entertainment Technology, Valencia, Spain, 15–17 June 2005. 2005. pp. 94-101

[41] Boulgouris NK, Hatzinakos D, Plataniotis KN. Gait recognition: A challenging signal processing technology for biometric identification. *IEEE Signal Processing Magazine*. 2005; 22:78-90

[42] Kimmeskamp S, Hennig EM. Heel to toe motion characteristics in Parkinson patients during free walking. *Clinical Biomechanics*. 2001;16:806-812

[43] Turcot K, Aissaoui R, Boivin K, Pelletier M, Hagemeister N, de Guise JA. New accelerometric method to discriminate between asymptomatic subjects and patients with medial knee osteoarthritis during 3-D gait. *IEEE Transactions on Biomedical Engineering*. 2008;55:1415-1422

[44] Bamberg SJM, Benbasat AY, Scarborough DM, Krebs DE, Paradiso JA. Gait analysis using a shoe-integrated wireless sensor system. *IEEE Transactions on Information Technology in Biomedicine*. 2008;12:413-423

[45] Choi JH, Cho J, Park JH, Eun JM, Kim MS. An efficient gait phase detection device based on magnetic

- sensor array. In: Proceedings of the 4th Kuala Lumpur International Conference on Biomedical Engineering, Vol. 21, Kuala Lumpur, Malaysia, 25–28 June 2008. 2008. pp. 778-781
- [46] Hidler J. Robotic assessment of walking in individuals with gait disorders. In: Proceedings of the 26th Annual International Conference of the IEEE Engineering in Medicine and Biology Society, Vol. 7, San Francisco, CA, USA, 1–5 September 2004. 2004. pp. 4829-4831
- [47] Wahab Y, Bakar NA. Gait analysis measurement for sport application based on ultrasonic system. In: Proceedings of the 2011 IEEE 15th International Symposium on Consumer Electronics, Singapore, 14–17 June 2011. 2011. pp. 20-24
- [48] ElSayed M, Alsebai A, Salaheldin A, El Gayar N, ElHelw M. Ambient and wearable sensing for gait classification in pervasive healthcare environments. In: Proceedings of the 12th IEEE International Conference on e-Health Networking Applications and Services (Healthcom), Lyon, France, 1–3 July 2010. 2010. pp. 240-245
- [49] Purwar A, Jeong DU, Chung WY. Activity monitoring from realtime triaxial accelerometer data using sensor network. In: Proceedings of International Conference on Control, Automation and Systems, Hong Kong, 21–23 March 2007. 2007. pp. 2402-2406
- [50] Software, Keysight. Available from: <http://www.keysight.com/en/pc-1297113/advanced-design-system-ads?cc=IL&lc=eng>
- [51] Pendry JB, Holden AJ, Stewart WJ, Youngs I. Extremely low frequency plasmons in metallic mesostructures. *Physical Review Letters*. 1996;76:4773-4776
- [52] Pendry JB, Holden AJ, Robbins DJ, Stewart WJ. Magnetism from conductors and enhanced nonlinear phenomena. *IEEE Transactions on Microwave Theory and Techniques*. 1999;47:2075-2084
- [53] Marque's R, Mesa F, Martel J, Medina F. Comparative analysis of edge and broadside coupled split ring resonators for metamaterial design. Theory and experiment. *IEEE Transactions on Antennas and Propagation*. 2003;51:2572-2581
- [54] Marque's R, Baena JD, Martel J, Medina F, Falcone F, Sorolla M, et al. Novel small resonant electromagnetic particles for metamaterial and filter design. In: Proceeding of the ICEAA'03, Torino, Italy. 2003. pp. 439-442
- [55] Marque's R, Martel J, Mesa F, Medina F. Left-handed-media simulation and transmission of EM waves in resonator-subwavelength split-ring-loaded metallic waveguides. *Physical Review Letters*. 2002;89:183901
- [56] Baena JD, Marque's R, Martel J, Medina F. Experimental results on metamaterial simulation using SRR-loaded waveguides. In: Proceedings of the IEEE-AP/S International Symposium on Antennas and Propagation, June 2003, Ohio USA. 2003. pp. 106-109
- [57] Marques R, Martel J, Mesa F, Medina F. A new 2-D isotropic left-handed metamaterial design: Theory and experiment. *Microwave and Optical Technology Letters*. 2002;35:405-408
- [58] Shelby RA, Smith DR, Nemat-Nasser SC, Schultz S. Microwave transmission through a two-dimensional, isotropic, left-handed metamaterial. *Applied Physics Letters*. 2001;78:489-491
- [59] Zhu J, Eleftheriades GV. A compact transmission-line Metamaterial antenna with extended bandwidth. *IEEE Antennas and Wireless Propagation Letters*. 2009;8:295-298